Solar Phys (2014) 289:951–976
DOI 10.1007/s11207-013-0375-8

Fundamental Emission of Type III Bursts Produced in Non-Maxwellian Coronal Plasmas with Kappa-Distributed Background Particles

B. Li · Iver H. Cairns

Received: 18 April 2013 / Accepted: 27 July 2013 / Published online: 29 August 2013

Abstract Detailed simulations based on quasi-linear theory are presented for fundamental (f_p) emission of type III bursts produced in non-Maxwellian, suprathermal, background coronal plasma by injection of energetic electrons during flares with a power-law or Maxwellian velocity distribution, where f_p is the electron plasma frequency. The background plasma is assumed to have a kappa (κ) distribution, as inferred from solar wind data and proposed by theories for the corona and solar wind. The predicted type III beam speeds, Langmuir wave levels, and the drift rate and flux of f_p emission are strongly sensitive to the presence of suprathermal background electrons in the corona. The simulations show the following results. i) Fast beams with speeds $v_b > 0.5c$ are produced for coronal background electrons with small κ ($\kappa \lesssim 5$) by injected electrons with power-law spectra. ii) Moderately fast beams with $v_b \approx 0.3-0.5c$ are generated in coronal plasma with $\kappa \lesssim 8$ by injections of power-law or Maxwellian electrons. iii) Slow beams with $v_b < 0.3c$ are produced for coronal background electrons with large κ ($\kappa > 8$), including the asymptotic limit $\kappa \to \infty$ where the electrons are Maxwellian, for both power-law and Maxwellian injections. The observation of fast type III beams (with $v_b > 0.5c$) thus suggests that these beams are produced in coronal regions where the background electron distribution has small κ by injected electrons with power-law spectra, at least when such beams are observed. The simulations, from the viewpoint of type III bursts, thus support: i) the presence, at least sometimes, of suprathermal background electrons in the corona and the associated mechanisms for coronal heating and solar wind acceleration; ii) power-law spectra for injected energetic electrons, consistent with observations of such electrons *in situ* and of X-ray emission.

Keywords Corona, radio emission · Corona: structures · Plasma physics · Radio bursts, theory · Radio bursts, type III

B. Li (✉) · I.H. Cairns
School of Physics, University of Sydney, Sydney, New South Wales, 2006, Australia
e-mail: boli@physics.usyd.edu.au

I.H. Cairns
e-mail: cairns@physics.usyd.edu.au

1. Introduction

Non-Maxwellian, suprathermal features of electron and ion velocity distribution functions are commonly observed in diverse space plasmas (Meyer-Vernet, 2001; Pierrard and Lazar, 2010). Examples include electron and ion distributions in the solar wind (Maksimovic, Pierrard, and Riley, 1997; Gloeckler, Geiss, and Fisk, 2001), planetary magnetospheres (Krimigis *et al.*, 1981; Gloeckler and Hamilton, 1987), and the outer heliosphere (*e.g.*, Decker *et al.*, 2005). The observed non-Maxwellian distributions have Maxwellian (thermal) cores and power-law tails, and are well parametrized by three-dimensional kappa (κ) (or generalized Lorentzian) distributions (Vasyliunas, 1968):

$$f_\alpha^\kappa(\mathbf{v}) = \frac{n_\mathrm{e}}{\pi^{3/2}} \frac{1}{\theta_\alpha^3} \frac{\Gamma(\kappa+1)}{\kappa^{3/2}\Gamma(\kappa-\frac{1}{2})} \left(1+\frac{v^2}{\kappa\theta_\alpha^2}\right)^{-(\kappa+1)}, \tag{1}$$

where

$$\theta_\alpha = \left(\frac{2\kappa-3}{\kappa}\right)^{1/2} v_\alpha, \tag{2}$$

κ ($>3/2$) is the spectral index, $\alpha = \mathrm{e}$ and $= \mathrm{i}$ are for electrons and ions, respectively, and $\Gamma(\kappa)$ is the gamma function. Here $\mathbf{v}$ denotes the velocity of a particle, $v_\alpha = (k_\mathrm{B}T_\alpha/m_\alpha)^{1/2}$ is the characteristic thermal speed, m_α and T_α are the mass and temperature of species α, respectively, and n_e is the plasma number density to which $f_\alpha^\kappa(\mathbf{v})$ is normalized via $\int \mathrm{d}\mathbf{v} f_\alpha^\kappa(\mathbf{v}) = n_\mathrm{e}$. In the limit $\kappa \to \infty$, the κ distribution becomes a Maxwellian distribution.

The observation of non-Maxwellian electron distributions in the solar wind suggests that suprathermal tails should also exist on the electron distributions in the background corona. The reason is that the electron mean free path in the solar wind is of the order of 1 AU (Scudder, 1992a; Maksimovic, Pierrard, and Riley, 1997); the distribution function should thus preserve its form from the corona to 1 AU. Indeed, values of $\kappa \approx 5-10$ were first inferred for electron distributions in the corona using ion charge states observed in the solar wind (Ko *et al.*, 1996). On the other hand, suprathermal distributions of coronal background particles have also been proposed in various coronal and solar wind models (Marsch, 2006; Pierrard and Lazar, 2010). For example, the "velocity filtration" model (Scudder, 1992a) predicts that the heating of the corona is a natural consequence of the existence of suprathermal background particles in the corona (Scudder, 1992b). Another example is the exospheric model, in which fast solar wind streams naturally form if the coronal background electrons have $\kappa = 2-3$, according to Pierrard and Lemaire (1996), Maksimovic, Pierrard, and Lemaire (1997).

Energetic electrons produced during flares and injected onto open magnetic field lines can produce type III solar radio bursts. These bursts drift rapidly from high to low frequencies; for example, the frequency drift rates for metric type III bursts are about 100 MHz s^{-1} (Suzuki and Dulk, 1985). On leaving the Sun fast electrons outrun slow ones and form beams, which generate Langmuir waves and radio emission near f_p and/or $2f_\mathrm{p}$ (Suzuki and Dulk, 1985; Bastian, Benz, and Gary, 1998; Pick and Vilmer, 2008). Here f_p is the local electron plasma frequency. In the corona type III beams have speeds of $v_\mathrm{b} \approx 0.1-0.6c$, with typical beam speeds of $\approx c/3$ (Suzuki and Dulk, 1985; Klassen, Karlicky, and Mann, 2003). Sometimes, even faster coronal type III beams with $v_\mathrm{b} \approx 0.6-0.8c$ are observed (Wild, Sheridan, and Neylan, 1959; Raoult *et al.*, 1989). Further, a subclass of type III bursts, type IIId bursts, are observed to have much larger drift rates than normal type III bursts

(Poquérusse, 1994; Klassen, Karlicky, and Mann, 2003; Liu *et al.*, 2009). It is commonly believed that type IIId bursts are produced by fast beams with $v_b \approx 0.5-1.0c$, where the beams propagate nearly along the line of sight towards the observer (Poquérusse, 1994; Klassen, Karlicky, and Mann, 2003). In contrast, v_b in the solar wind is lower and ranges from $\approx 0.03c$ to $0.25c$ (Fainberg, Evans, and Stone, 1972; Lin *et al.*, 1981; Dulk *et al.*, 1987; Graham *et al.*, 2012).

Recently, large-scale, kinetic simulations of coronal type III bursts based on the quasi-linear theory have been developed, predicting both phenomena in the radiation source and the radiation observed remotely (*e.g.*, Li, Cairns, and Robinson, 2008a; Li and Cairns, 2012). The simulation predictions of type III spectral characteristics, *e.g.*, drift rate and brightness temperature, agree quantitatively with typical observations, for type III bursts with unidirectional (*e.g.*, Li, Cairns, and Robinson, 2008b, 2009) or bidirectional (Li, Robinson, and Cairns, 2008; Li *et al.*, 2011) drift morphologies, and for type III bursts perturbed by shocks (Li and Cairns, 2012). However, the predicted type III beams have $v_b \lesssim 0.25c$ when the background plasma is Maxwellian, and these v_b values thus correspond to the lower half of the observed range. This result is found whether the injected electrons have power-law velocity distribution (Li and Cairns, 2013b) or Maxwellian velocity distribution (*e.g.*, Li, Cairns, and Robinson, 2008b; Li, Robinson, and Cairns, 2008). Consequently, our simulations suggest that electron beams produced in a Maxwellian-distributed coronal plasma can only account for relatively slow coronal type III beams, and are unable to explain the often observed fast beams.

Motivated by observations that often coronal type III bursts have $v_b > 0.3c$ and that type IIId bursts have much larger v_b, and by the inferences and suggestions that the coronal background particles are generally suprathermal, here we present the first detailed, quasi-linear-based simulations of coronal type III bursts assuming that the background electrons and ions have κ distributions. Specifically, we simulate in detail f_p emission produced in the corona and observed remotely at Earth, by injecting energetic electrons associated with flares onto open magnetic field lines embedded in a κ background corona, extending our initial calculations (Li and Cairns, 2013a). We find that the predicted type III bursts show both qualitative and quantitative differences from those when the background particles are Maxwellian-distributed. i) Fast beams with $v_b \gtrsim 0.5c$ can be produced for $\kappa \lesssim 5$ and injected electrons with power-law spectra (Li and Cairns, 2013a). ii) For the same injected electrons, beams produced in plasmas with κ background electrons are faster than those with Maxwellian background electrons, irrespective of the detailed spectral forms (power-law or Maxwellian) of the injected electrons. iii) For f_p emission with similar onset frequencies, the emission generated in a κ plasma has faster increase in flux with decreasing frequency than in a Maxwellian plasma. Therefore, a κ-distributed coronal plasma favors such f_p emission to be remotely observed, despite severe losses by free-free absorption and scattering-induced damping (*e.g.*, Robinson and Cairns, 1998; Benz, 2002; Li, Cairns, and Robinson, 2008a). In contrast, previous simulations (*e.g.*, Li, Cairns, and Robinson, 2009) show that in a Maxwellian-distributed corona the fluxes of f_p radiation reaching Earth should be low and only marginally observable.

These new results demonstrate observable manifestations of crucial modifications to the physics of type III bursts due to the presence of suprathermal background particles in the corona. We find that in a κ-distributed background corona, the electron beam, beam-Langmuir wave interactions, and nonlinear wave-wave interactions that lead to emission of type III bursts take place primarily at larger phase speeds and smaller wavenumbers than in a Maxwellian plasma. The new results may resolve longstanding issues regarding the speeds of coronal type III beams and the production of remotely observable levels of f_p emission despite heavy losses in the corona. The simulations also suggest that the distributions

of coronal background electrons should be κ-like (with $\kappa \lesssim 5$) and the injected electrons should have power-law spectra, at least when type III bursts associated with fast beams ($v_b > 0.5c$) are observed.

The simulation model is discussed in Section 2. We first introduce in detail the modifications to Langmuir and ion sound waves involved in type III emission, due to changes from Maxwellian to κ distributions of background electrons and ions. Then we review briefly our previous model for the type III bursts in Maxwellian background plasmas, and generalize the model to κ-distributed background plasmas for f_p emission. However, here we do not predict the $2f_p$ emission, due to model limitations discussed in Sections 2.2 and 6. Section 3 shows the simulations with power-law injected electrons for two illustrative cases with $\kappa = 5$ and 7, which are compared with a third case in which the background plasma is the corresponding Maxwellian type. The f_p radiation predicted at Earth is studied in detail, as are the electron beams, Langmuir waves, and the radiation predicted in the radio sources. Section 4 studies the effects on the spectral properties of f_p emission and the beam speed of varying the κ index, for the same power-law injection as in Section 3. Section 5 presents the predictions for f_p emission for injected electrons with Maxwellian spectra and compares the results with those for power-law injection. Section 6 discusses the results and implications of the simulations, as well as future improvements. The conclusions are presented in Section 7.

2. Model for Predicting Type III Bursts in κ-Distributed Corona

We assume that electrons and ions in the background corona have isotropic three-dimensional κ velocity distributions with the same κ index (Pierrard and Lazar, 2010). Section 2.1 discusses the modifications to Langmuir and ion sound waves due to the presence of suprathermal background particles. Section 2.2 reviews the original type III model for Maxwellian background plasmas (Li, Cairns, and Robinson, 2008a; Li, Robinson, and Cairns, 2008) and generalizes it to κ background plasmas.

2.1. Electrons, Langmuir, and Ion Sound Waves in a κ-Distributed Plasma

The one-dimensional distribution function $f_{1D}^{\kappa}(v)$ corresponding to the three-dimensional $f_{\alpha}^{\kappa}(\mathbf{v})$ in Equation (1) is given by (Summers and Thorne, 1991)

$$f_{1D}^{\kappa}(v) = \frac{n_e}{\pi^{1/2}} \frac{1}{\theta} \frac{\Gamma(\kappa+1)}{\kappa^{3/2}\Gamma(\kappa-1/2)} \left(1 + \frac{v^2}{\kappa\theta^2}\right)^{-\kappa}, \tag{3}$$

where v now denotes the component of $\mathbf{v}$ along the magnetic field, and we have omitted the subscript α to simplify the notation.

In a κ-distributed plasma the Langmuir dispersion relation is (Thorne and Summers, 1991)

$$\omega_L^2 = \omega_p^2 + 3k^2 {v_e}^2, \tag{4}$$

where $\omega_p = (n_e e^2/m_e\varepsilon_0)^{1/2}$ is the electron plasma frequency, and k is the wavenumber of a Langmuir wave. Equation (4) thus has the same form as in a Maxwellian plasma. However, the ion sound dispersion relation is modified as (Thorne and Summers, 1991; Zaheer, Murtaza, and Shah, 2004)

$$\omega_S = \left(\frac{\kappa - 1/2}{\kappa - 3/2} + \bar{k}^2\right)^{-1/2} k c_S, \tag{5}$$

where $c_S = [(1 + \sqrt{1 + 12T_i/T_e})k_B T_e/(2m_i)]^{1/2}$ is the ion sound speed (Cairns, 2000), $\bar{k} = k/k_D$, and $k_D = \omega_p/v_e$ is the electron Debye wavenumber.

The rate $\alpha_M(k)$ of spontaneous emission for wave mode M, with M = L and S for Langmuir and ion sound waves, respectively, in a κ-distributed plasma can be obtained by using three-dimensional particle distribution functions (Melrose, 1986). Specifically, we have (see the Appendix)

$$\alpha_L(k) = \left(\frac{\pi}{2}\right)^{1/2} \frac{k_B T_e}{4\pi\hbar} \left(\frac{\omega_L}{\omega_p}\right)^3 \frac{(k_D^2 - k^2)}{|\bar{k}|^3} \frac{\Gamma(\kappa+1)}{\kappa(\kappa-3/2)^{1/2}\Gamma(\kappa-1/2)} \times \left[1 + \left(\frac{1}{2\bar{k}^2} + \frac{3}{2}\right)\frac{1}{\kappa-3/2}\right]^{-\kappa}, \tag{6}$$

$$\alpha_S(k) = \left(\frac{\pi}{2}\right)^{1/2} \frac{k_B T_e}{4\pi\hbar} \left(\frac{T_e}{T_i}\right)^{1/2} \frac{(k_D^2 - k^2)}{(1+|\bar{k}|^2)^{3/2}} \frac{\Gamma(\kappa+1)}{\kappa(\kappa-3/2)^{1/2}\Gamma(\kappa-1/2)} \times \left\{\left(\frac{m_e T_i}{m_i T_e}\right)^{1/2} + \left[1 + \frac{T_e/T_i}{2(1+\bar{k}^2)}\frac{1}{\kappa-3/2}\right]^{-\kappa}\right\}. \tag{7}$$

The thermal wave levels $N_{M\theta}(k)$ are calculated by balancing the spontaneous emission and Landau damping via (Melrose, 1986)

$$N_{M\theta}(k) = \alpha_M(k)/\gamma_M(k), \tag{8}$$

where γ_M is the thermal Landau damping rates. In a κ-distributed plasma, we have (Zaheer, Murtaza, and Shah, 2004):

$$\gamma_L(k) = \left(\frac{\pi}{2}\right)^{1/2} \frac{\omega_L}{\bar{k}^3} \frac{\Gamma(\kappa+1)}{(\kappa-3/2)^{3/2}\Gamma(\kappa-1/2)} \left[1 + \frac{1}{(2\kappa-3)\bar{k}^2} + \frac{3}{2\kappa-3}\right]^{-(\kappa+1)}, \tag{9}$$

$$\gamma_S(k) = \left(\frac{\pi}{2}\right)^{1/2} \left(\frac{T_e}{T_i}\right)^{3/2} \frac{\omega_S}{[1+(1+\bar{k}^2)(\kappa-3/2)]^{3/2}} \frac{\Gamma(\kappa+1)}{\Gamma(\kappa-1/2)} \times \left\{\left(\frac{m_e}{m_i}\right)^{1/2} \left(\frac{T_i}{T_e}\right)^{3/2} + \left[1 + \frac{T_e/T_i}{2[1+(1+\bar{k}^2)(\kappa-3/2)]}\right]^{-(\kappa+1)}\right\}, \tag{10}$$

for Langmuir and ion sound waves, respectively.

2.2. Simulation Model for Type III Bursts

We assume that type III bursts are produced by plasma emission mechanisms (*e.g.*, Suzuki and Dulk, 1985; Bastian, Benz, and Gary, 1998). Alternative mechanisms, *e.g.*, linear mode conversion (Kim, Cairns, and Robinson, 2008), antenna emission (Malaspina, Cairns, and Ergun, 2010), and non-gyrotropic beam-driven emission (Tsiklauri, 2011), are assumed to be unimportant and so are not included. Specifically, our model (Li, Cairns, and Robinson, 2008a; Li, Robinson, and Cairns, 2008) assumes that the following processes produce the radiation (*e.g.*, Melrose, 1986; Cairns, 1987a, 1987b; Robinson and Cairns, 1993, 1998): ($\mathcal{A}$) growth of Langmuir (L) waves due to the bump-on-tail beam instability and quasi-linear interaction with the beam; ($\mathcal{B}$) generation of backscattered Langmuir (L') waves and forward-going ion sound (S) waves by electrostatic (ES) decay $L \rightarrow L' + S$ of L waves; ($\mathcal{C}$) production of f_p radiation (F waves) and ion sound (S') waves by electromagnetic (EM)

decay $L \rightarrow F + S^{'}$ of L waves; and ($\mathcal{D}$) generation of $2f_{\rm p}$ radiation (H waves) due to coalescence $L + L^{'} \rightarrow H$ of L and $L^{'}$ waves.

The model (Li, Cairns, and Robinson, 2008a) simulates the temporal (t) and spatial (x) evolutions of electrons, L and S waves, and radiation in a three-dimensional source region whose two-dimensional layers are stratified and vary with x along a magnetic field line (assumed to be radial), where $x = r - R_{\odot}$ is the radial distance above the photosphere. Specifically, the model predicts the evolution of the electron distribution function $f_{\rm e}(t, x, v)$ and the occupation numbers $N_{\rm M}(t, x, v)$ (M = L or S) for Langmuir and ion sound waves following the quasi-linear equations that incorporate the processes ($\mathcal{A}$) and ($\mathcal{B}$) above. The emission rates $\Gamma_{\rm T}(t, x, f, k_{\rm T}, \chi)$ for transverse waves (T = F or H) are calculated using $N_{\rm L}(t, x, v)$ and $N_{\rm S}(t, x, v)$. Here f and $k_{\rm T}$ are the frequency and wavenumber of the radiation, respectively, and χ is the emission angle relative to the direction of beam propagation. The model then predicts the type III dynamic spectra at Earth, *i.e.*, the radio fluxes $\Phi_{\rm F}(t, f)$ and $\Phi_{\rm H}(t, f)$ for $f_{\rm p}$ and $2f_{\rm p}$ emission, respectively. For example, for $f_{\rm p}$ emission we have (Li, Cairns, and Robinson, 2008a)

$$\Phi_{\rm F}(t, f) = \sum_{t_{\rm s}} \sum_{x_{\rm s}} \int {\rm d}\chi \sin\chi C_{\rm F}(t, f; \chi) \int {\rm d}k_{\rm F} \left[k_{\rm F}^2 \Gamma_{\rm F}(t_{\rm s}, x_{\rm s}, f, k_{\rm F}, \chi)\right], \tag{11}$$

where $x_{\rm s}$ is the source location at time $t_{\rm s}$. The coefficient $C_{\rm F}$ is independent of $k_{\rm F}$ but dependent on t, f, details of the source (*e.g.*, $x_{\rm s}$, χ, distance between the source and observer), and the effects of absorption (*e.g.*, Benz, 2002) and scattering (*e.g.*, Riddle, 1974; Robinson and Cairns, 1998) during propagation from the source to Earth. The quantitative detail of $C_{\rm F}$ is defined through Equations (1), (4), (17), and (18) in Li, Cairns, and Robinson (2008a). The functional form of the $k_{\rm F}$-integral in Equation (11) shows that, when relating $f_{\rm p}$ emission observed remotely to its source, the weighted emission rate $k_{\rm F}^2 \Gamma_{\rm F}$, not the actual rate $\Gamma_{\rm F}$, should be studied in detail.

Our original model (Li, Cairns, and Robinson, 2008a; Li, Robinson, and Cairns, 2008) assumed Maxwellian distributions for the background electrons and ions, following previous simulations (*e.g.*, Magelssen and Smith, 1977; Grognard, 1985; Kontar, 2001; Ziebell, Gaelzer, and Yoon, 2001). The current work generalizes this model, now allowing the background particles to have κ distributions and including the effects of κ distributions on the damping, thermal levels, and spontaneous emission of L and S waves discussed in Section 2.1. As often adopted, our model assumes the cold plasma approximation (*e.g.*, Melrose, 1986) for the wave-wave interactions, *i.e.*, assuming that the nonlinear processes ($\mathcal{B}$)–($\mathcal{D}$) do not explicitly depend on the background particle distributions. This assumption is well satisfied for $2f_{\rm p}$ emission in the corona; for example, Layden *et al.* (20011) showed that thermal corrections to the $2f_{\rm p}$ emission rate are negligible when the speeds v of beam electrons satisfy $v > 3v_{\rm e}$, a condition that is well met here. Nonetheless, these processes do depend sensitively, via the properties (levels and wavenumbers) of L and S waves, on the quantitative details of the beam distributions (Li *et al.*, 2005a, 2005b). Section 3 shows that the beam distributions are significantly modified for coronal conditions by the presence of suprathermal particles in κ plasmas, as are the Langmuir waves and $f_{\rm p}$ emission.

Note that we do not study $2f_{\rm p}$ emission in this work, because of significant changes in the kinematics of the process ($\mathcal{D}$), *i.e.*, $L + L^{'} \rightarrow H$, between the current simulations and our previous simulations for Maxwellian background corona (with Maxwellian spectra for the injected electrons) (*e.g.*, Li *et al.*, 2005a; Li, Cairns, and Robinson, 2008b). Specifically, some beam electrons in the current simulations are too fast for the L and $L^{'}$ waves to meet the "head-on" approximation (*e.g.*, Cairns, 1987b; Willes, Robinson, and Melrose, 1996)

that is assumed in our original model (Li *et al.*, 2005a; Li, Cairns, and Robinson, 2008a). Further discussion of the $2f_p$ emission is deferred to Section 6.

3. Simulations with Representative κ Indices for Power-Law Electron Injection

Simulation predictions for f_p emission generated in κ plasmas are presented in this section for two representative values of κ, when the injected electrons have a power-law spectrum. The predictions are compared with those for the corresponding Maxwellian plasma and otherwise identical simulation conditions. We first introduce the simulation parameters; then in Section 3.2 we present the predicted f_p emission observable at Earth, and in Section 3.3 the diagnostics inside the coronal type III sources.

3.1. Simulation Parameters

We present simulations with $\kappa = 5$ (simulation 1 or S1) and $\kappa = 7$ (S2) in order to demonstrate the effects on type III bursts of the coronal background electrons and ions with κ distributions. Both κ indices fall within the range inferred by Ko *et al.* (1996). The two simulations are compared with a third simulation (S3), where the background plasma is the corresponding Maxwellian, *i.e.*, the same n_e, T_e, and T_i, but where $\kappa \to \infty$ in Equation (3). For S1 – S3 all the other simulation parameters discussed below are the same.

We assume that the corona has a smooth, fourfold Baumbach–Allen density profile (Allen, 1947) and is isothermal with $T_e = T_i = 2$ MK. The energetic electrons produced during a flare are represented via a broken power-law spectrum, according to X-ray observations (Lin, 1974, 2011):

$$I_p(v) = \frac{p-1}{pv_0} \begin{cases} 1, & v < v_0, \\ (v_0/v)^p, & v \geq v_0, \end{cases} \tag{12}$$

where v_0 is the break speed. The spectrum $I_p(v) \propto v^{-p}$ for $v \geq v_0$ with a spectral index p, and is flat elsewhere. We assume $p = 5$ and $v_0 = 7 \times 10^7$ m s^{-1}, within the ranges used in previous modeling (*e.g.*, Magelssen and Smith, 1977; Reid, Vilmer, and Kontar, 2011). These electrons are injected onto an open magnetic field line and are modeled by adding a source term S to the equation for electron evolution (*e.g.*, Li, Cairns, and Robinson, 2008a, 2011):

$$\frac{\partial f_e}{\partial t} + v\frac{\partial f_e}{\partial x} = \frac{\partial}{\partial v}(Af_e) + \frac{\partial}{\partial v}\left(D\frac{\partial f_e}{\partial v}\right) + Q(x,v) + S(t,x,v), \tag{13}$$

where

$$S(t,x,v) = \frac{F_{inj}}{\sqrt{\pi}\delta t} I_p(v) \exp\left[-\frac{(t-t_0)^2}{(\delta t)^2} - \frac{(x-x_0)^2}{(\delta x)^2}\right]. \tag{14}$$

The first and second terms on the right-hand side of Equation (13) represent spontaneous and induced emission, respectively, and the third term Q self-consistently maintains the inhomogeneous profiles $f_{1D}^{\kappa}(x,v)$, $n_e(x)$, and $T_e(x)$ of the background plasma (Li, Cairns, and Robinson, 2011). The source electrons cause the formation of a type III beam due to time-of-flight effects. The injection [Equation (14)] is localized in time and position with Gaussian profiles, centered at time $t = t_0$ after the start of the simulations and at a height $x = x_0$, over a characteristic spatiotemporal domain of δt and δx. The total number of injected electrons is a fraction F_{inj} ($\ll 1$) of the background electrons. We parametrize the

Table 1 Summary of parameters (columns 2 – 5) characterizing simulations S1 – S3 in Section 3, S4 in Section 4, and S5 in Section 5, and the predicted beam speed v_b/c (column 6). The simulations are characterized by κ in Equation (3) for the background particle distribution functions and by the spectral form, *i.e.*, power-law [Equation (12)] or Maxwellian [Equation (16)], and the fraction F_{inj} in Equation (14) for the injected energetic electrons. Here $p = 5$ and $v_0 = 7 \times 10^7$ m s^{-1} for the power-law spectrum, and $T_h = 30$ MK for the Maxwellian spectrum.

Simulation ID	Background κ	Particle injection			Beam speed v_b/c
		Power-law	Maxwellian	F_{inj}	
S1	5	Y	–	5×10^{-6}	0.58
S2	7	Y	–	5×10^{-6}	0.35
S3	∞	Y	–	5×10^{-6}	0.25
S4	5	Y	–	5×10^{-5}	0.45
S5	5	–	Y	5×10^{-5}	0.30

source based on observations, with $\delta t = 2$ ms and $\delta x = 3$ Mm (Aschwanden, 2002), and $x_0 = 0.108$ Gm (Klein *et al.*, 2005). The injection is centered at $t_0 = 50$ ms after the beginning of S1 – S3. The parameter F_{inj} is chosen to be 5×10^{-6}, based on our earlier work for Maxwellian background plasmas (*e.g.*, Li, Cairns, and Robinson, 2008b). Table 1 summarizes the parameters characterizing simulations S1 – S3 here and the other simulations in Sections 4 and 5. It also lists the beam speeds v_b/c obtained, as discussed in detail, for example, for S1 – S3 in Sections 3.2 and 3.3.

Besides large-scale regular density variations, small-scale density fluctuations are ubiquitous in the corona (Coles and Harmon, 1989). The fluctuations scatter f_p emission leaving its source, causing time delays and losses of the radiation reaching the observer (*e.g.*, Riddle, 1974; Robinson and Cairns, 1998). These scattering effects are included in our simulations (Li, Cairns, and Robinson, 2008a), by using two characteristic parameters of the fluctuations: the RMS level $\delta n_e/n_e$ and the mean length scale l. We assume parametrizations similar to our previous work for both $\delta n_e/n_e$ and l, since no observational data are available for the coronal region ($r < 2R_\odot$) of interest here. Specifically, we assume constant $\delta n_e/n_e = 1$ % (*e.g.*, Steinberg *et al.*, 1971; Thejappa and MacDowall, 2008) and increasing l with x (*e.g.*, Steinberg *et al.*, 1971; Subramanian and Cairns, 2011) via $l(x) = 10^5[(x + R_\odot)/1\ \mathrm{AU}]^{1.61}$ m (Robinson and Cairns, 1998). The f_p emission at the observer depends sensitively on both parameters, as discussed previously (*e.g.*, Robinson and Cairns, 1998; Li, Cairns, and Robinson, 2009).

3.2. Remote Radiation

Figure 1 shows, for S1 – S3, the predicted f_p dynamic spectra $\Phi_F(t, f)$, the frequency profiles of the maximum flux $\Phi_F^{max}(f)$, and the corresponding frequency drift rate $\mathrm{d}f/\mathrm{d}t$. We see from Figures 1(a) – 1(c) that for S1 – S3 the flux levels of f_p emission increase with decreasing f and are above the thresholds ($\gtrsim 1$ sfu $= 10^{-22}$ W m^{-2} Hz^{-1}) of typical instruments, at least for the lower range of the simulated frequencies. The predicted f_p emission for all three different background conditions is thus observable. Nevertheless, the radio burst in Figure 1(a) for $\kappa = 5$ is weakest and that in Figure 1(c) for the Maxwellian background is strongest. Figure 1(d) further shows that for S1 – S3 Φ_F^{max} increases with decreasing f at similar (approximately) exponential rates. The predicted $\Phi_F^{max}(f)$ levels and trends agree with typical observations (*e.g.*, Suzuki and Dulk, 1985).

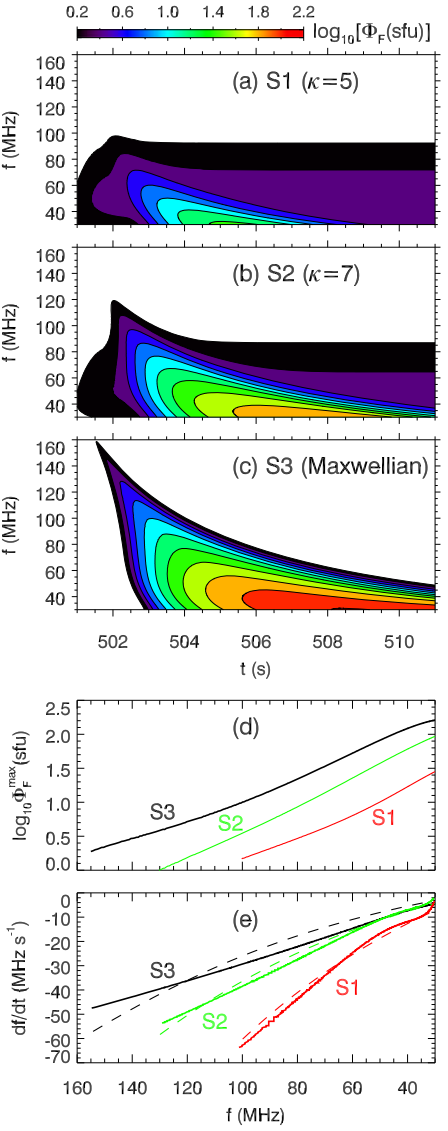

Figure 1 Predicted dynamic spectra of f_p emission and the corresponding frequency profiles of spectral characteristics for S1 – S3. Dynamic spectra (a) S1: $\kappa = 5$, (b) S2: $\kappa = 7$, and (c) S3: Maxwellian. Frequency profiles of (d) Φ_F^{max} and (e) df/dt for S1 (red), S2 (green), and S3 (black). The corresponding dashed curves in (e) are the predictions of Equation (15) for $v_b = 0.58c$, $0.35c$, and $0.25c$, respectively.

The frequency profiles of the maximum brightness temperature T_b^{max} (not shown; *cf.* Li, Cairns, and Robinson, 2009) follow closely those of Φ_F^{max} in Figure 1(d), for S1 – S3. The similar trends of variations between the two quantities occur because $T_b(f) \propto (R/Df)^2 \Phi_F(f)$ (Benz, 2002; Li, Cairns, and Robinson, 2008a), where D is the source diameter and R is the source distance from the observer. Here D, R, and f vary within the simulated domain relatively weakly compared to the $\Phi_F^{max}(f)$ variations so that the profiles of $T_b^{max}(f)$ resemble approximately those of $\Phi_F^{max}(f)$, as found in our earlier work (*e.g.*, Li, Robinson, and Cairns, 2008; Li, Cairns, and Robinson, 2009). Moreover, the predicted T_b^{max} values fall within yet near the lower bound of typical observations (Suzuki and Dulk, 1985, and references therein). For example, for S2, $T_b^{max} = 3.4 \times 10^7$ K and 4.9×10^9 K at $f = 130$ MHz and 30 MHz, respectively.

Figure 1(e) shows that the simulated $\mathrm{d}f/\mathrm{d}t$ are quantitatively different among the three cases. Specifically, the burst in S1 drifts fastest from high to low f, although it is weakest among the three bursts in Figures 1(a) – 1(c). In contrast, the burst produced in the Maxwellian background drifts slowest but is strongest. For example, for S1, $\mathrm{d}f/\mathrm{d}t \approx -64$ MHz s^{-1} at $f = 100$ MHz, which is about twice as large in magnitude as the corresponding result for S3. Figure 1(e) also shows the $\mathrm{d}f/\mathrm{d}t$ results predicted according to the plasma emission scenario. It is well known that there exists a quantitative relation between the type III drift rate $\mathrm{d}f/\mathrm{d}t$ and the beam speed v_b characterizing the type III beam (Wild, 1950):

$$\frac{\mathrm{d}f}{\mathrm{d}t} = \frac{v_\mathrm{b}}{2}\frac{\mathrm{d}(\ln n_\mathrm{e})}{\mathrm{d}x} f, \tag{15}$$

where v_b is assumed to be constant. For the same density profile in S1 – S3 we see that the predicted $\mathrm{d}f/\mathrm{d}t$ agree well with the simulated results for S1 and S2, but less well for S3 (Li, Cairns, and Robinson, 2008b), assuming $v_\mathrm{b} = 0.58c$, $0.35c$, and $0.25c$ for S1, S2, and S3, respectively. We will show in Section 3.3 that these v_b values are consistent with the speeds and dynamics of beam electrons in the sources. Therefore, Equation (15) applies well to the f_p emission produced in the κ plasmas. More significantly, the drift rates of the remotely observed radiation indicate that the type III beams produced in the κ plasmas are faster than in the Maxwellian plasma with the same n_e and T_e profiles, with v_b reaching $\approx 0.6c$ for $\kappa = 5$, which is well above the value for the Maxwellian plasma. Therefore, coronal type III beams with $v_\mathrm{b} > c/3$ are naturally produced here in S1 and S2.

Since the propagation of radiation is independent of the microscopic details of the background particle distributions (Li, Cairns, and Robinson, 2008a), the propagation effects on f_p emission are the same for S1 – S3. Consequently, the differences in the remotely observed f_p emission between the κ and Maxwellian plasmas in Figure 1 are attributed to changes inside the radiation sources. This is confirmed below.

3.3. Radiation Source

As discussed in Section 2.2, when considering source contributions to the remotely observed f_p emission, the directly relevant quantity is the weighted emission rate $k_\mathrm{F}^2\Gamma_\mathrm{F}$ per Equation (11). Thus a detailed comparison of this quantity near its peak between the κ and Maxwellian plasmas will yield insight into the origins of the changes in $\Phi_\mathrm{F}^\mathrm{max}$, $\mathrm{d}f/\mathrm{d}t$, and v_b among the three cases in Section 3.2. We therefore study here $k_\mathrm{F}^2\Gamma_\mathrm{F}$ near its maximum at specific times $t_\mathrm{a} = 1.3$ s, 1.7 s, and 1.9 s for S1, S2, and S3, respectively, at a sample frequency $f_\mathrm{p} = 82$ MHz, which originates from a specific location $x_\mathrm{a} = 0.302$ Gm in the source region. Figure 2 shows, for S1 – S3, $k_\mathrm{F}^2\Gamma_\mathrm{F}(k_\mathrm{F}, \chi)$ at t_a and x_a, and the corresponding Langmuir wave occupation number $N_\mathrm{L}(x, v)$ and electron distribution function $f_\mathrm{e}(x, v)$ at t_a, which are chiefly responsible for the production of f_p emission and Langmuir waves, respectively. (The variations of the ion sound waves are unimportant because they are essentially thermal, due primarily to strong damping associated with $T_\mathrm{e}/T_\mathrm{i} = 1$, and so are not shown. Further discussion of these waves is deferred to Section 6.) Below we focus on comparisons of the results between S1 and S3. The results for S2 fall between S1 and S3 and so follow easily. To aid understanding of the results in Figure 2, we further show in Figure 3, for S1 – S3 and $x = x_\mathrm{a}$, the background electron distribution function $f_\mathrm{1D}^\kappa(v)$ and the associated Landau damping rate $\gamma_\mathrm{L}(v)$ of Langmuir waves, given by Equations (3) and (9), respectively.

We see from Figures 2(a) – 2(c) that the following substantial differences in $f_\mathrm{e}(x, v)$ exist between the three simulations. i) Significantly different background plasmas are experienced

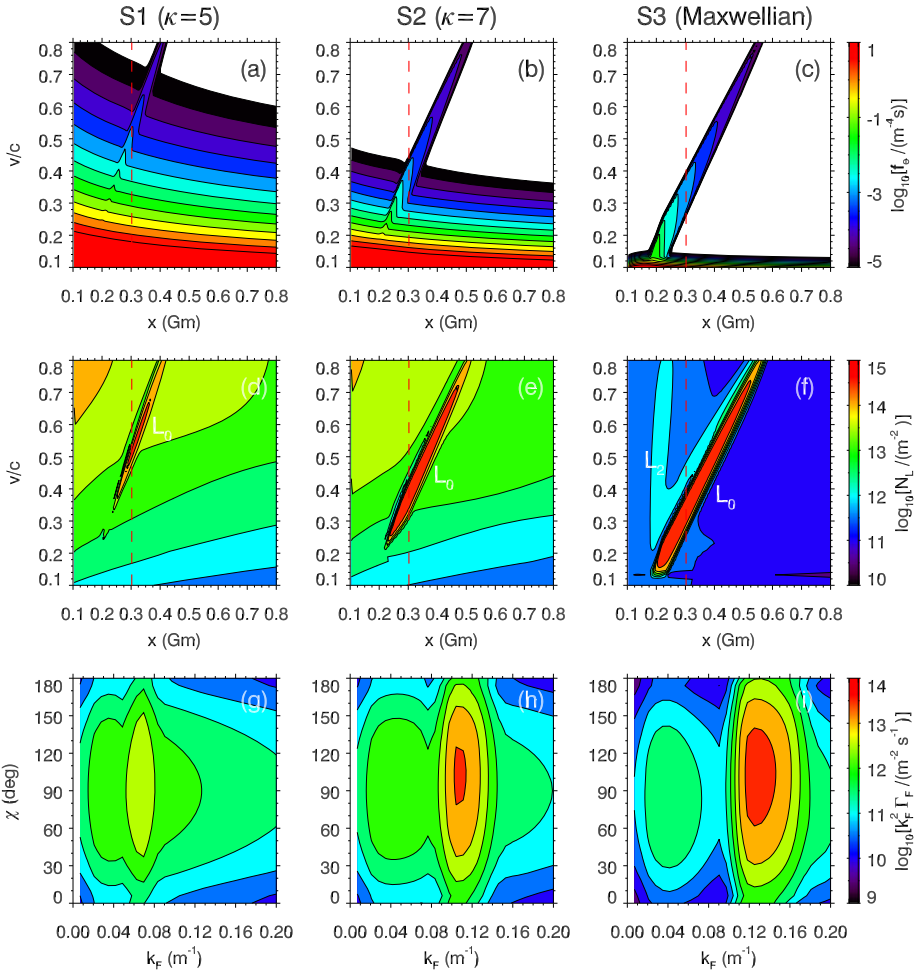

Figure 2 Beam and waves in source regions for S1 (left), S2 (middle), and S3 (right) at times $t_a = 1.3$ s, 1.7 s, and 1.9 s, respectively, when the weighted f_p emission rate $k_F^2\Gamma_F$ maximizes at $f_p(x_a = 0.302\ \text{Gm}) = 82$ MHz. Rows 1 and 2: phase space distributions $f_e(x, v)$ and $N_L(x, v)$ of electrons and Langmuir waves, respectively. Dashed lines in (a)–(f) indicate $x = x_a$. Row 3: $k_F^2\Gamma_F$ at x_a as a function of k_F and χ.

by the three beams. This is expected, since Figure 3(a) shows that $f_{1D}^{\kappa=5}(v)$ is larger than $f_{1D}^{\kappa\to\infty}(v)$ by many orders of magnitude for $v \gg v_e = 0.018c$, *e.g.*, by more than 19 orders of magnitude at $v = 0.2c$, and much more at larger v. ii) At a given location, the beam in Figure 2(a) is fastest and that in Figure 2(c) is slowest. For example, at $x = x_a$ the speeds of the beam electrons range from $v_{min} \approx 0.46c$ to $v_{max} \approx 0.55c$ in Figure 2(a), and from $0.26c$ to $0.4c$ in Figure 2(c). Here v_{min} and v_{max} are the minimum and maximum speeds, respectively, of the beam electrons for which a positive slope, *i.e.*, $\partial f_e/\partial v > 0$, exists. The larger v_{min} and v_{max} for S1 occur because for S1 the beam electrons reach x_a earlier (at $t_a = 1.3$ s) than for S3 (at $t_a = 1.9$ s). Kinematically, the beam electrons at x_a in Figure 2(a) are thus faster than in Figure 2(c). Moreover, the beam speed $v_b \approx 0.58c$ for S1 obtained from Figure 1(e) agrees well with $v_{max} \approx 0.55c$ in Figure 2(a), as for S3 with $v_b \approx 0.25c$

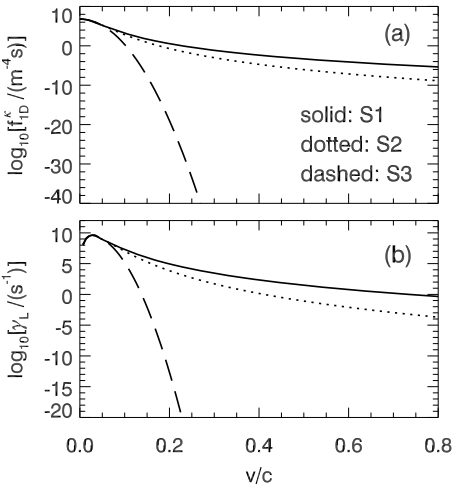

Figure 3 Variations with v at $x_a = 0.302$ Gm of (a) the background electron distribution functions $f^{\kappa}_{1D}(v)$ and (b) the corresponding Landau damping rates γ_L for Langmuir waves, for S1 (solid), S2 (dotted), and S3 (dashed).

and $v_{min} \approx 0.26c$. Thus, for coronal plasmas with κ distributions, the v_b values inferred from the dynamic spectra of f_p emission (*e.g.*, from Figure 1) are consistent with the speeds and dynamics of beam electrons in the source, as found earlier for Maxwellian background distributions (*e.g.*, Li, Cairns, and Robinson, 2008b; Li and Cairns, 2013b).

Figures 2(d) – 2(f) show that beam-driven Langmuir (L_0) waves are generated at phase speeds v that are the speeds of beam electrons in Figures 2(a) – 2(c). This occurs mainly due to the standard bump-on-tail instability, with the wave levels limited by competition between linear growth/damping and quasi-linear relaxation (*e.g.*, Grognard, 1985). We see from Figure 3(b) that γ_L is markedly different between S1 and S3, being substantially larger for S1, except for very small v ($\lesssim 3v_e$). This is expected because of the very different background $f^{\kappa}_{1D}(v)$ in Figure 3(a). In competing with the beam growth rate, the very large Landau damping rate in S1 tends to reduce or prevent growth of L_0 waves (if these waves can grow at all). The effects of ES decays on the levels of L_0 waves are much weaker than the linear and quasi-linear effects, since the produced Langmuir waves are at diminished levels (Ziebell, Gaelzer, and Yoon, 2001; Kontar and Pecseli, 2002; Li *et al.*, 2003). For example, weak nonthermal produced Langmuir waves are found in S3 but not in S1 and S2. Figure 2(f) shows the enhancement of very weak L_2 waves near $x \approx 0.2$ Gm. These waves are produced by ES decay $L_1 \rightarrow L_2 + S_\theta$, where the L_1 waves (with $v < 0$, not shown) are generated by the first ES decay $L_0 \rightarrow L_1 + S_\theta$. Here S_θ stands for thermal ion sound waves.

Figures 2(g) – 2(i) show that $k_F^2 \Gamma_F$ is approximately symmetric about and maximizes near $\chi = 90°$, as in previous work (*e.g.*, Li *et al.*, 2005b; Li, Cairns, and Robinson, 2008b). We see that the dominant emission peaks at $k_F \approx 0.07$ m^{-1}, 0.11 m^{-1}, and 0.13 m^{-1} for S1, S2, and S3, respectively, with the peak rate for S3 being largest. The emission is F_1 waves generated by EM decay $L_0 \rightarrow F_1 + S_\theta$ of the L_0 waves in Figures 2(d) – 2(f), where the L_0 waves in Figure 2(f) for S3 are strongest. The smaller k_F for smaller κ (*e.g.*, with k_F for S1 about half of that for S3) results from two factors: first, $k_L(L_0) = \omega_L / v(L_0)$ is smaller because $v(L_0)$ is larger for smaller κ, as discussed above, and, second, k_F is linearly proportional to k_L (Cairns, 1987a; Li *et al.*, 2005b). Figure 2(g) also shows a much weaker peak at smaller $k_F \approx 0.04$ m^{-1}, where the emission is F_2 waves produced by another EM decay $L_1 \rightarrow F_2 + S_\theta$.

In order to further understand the changes in the beam dynamics and the remote f_p emission between the κ and Maxwellian plasmas, Figure 4 contrasts the temporal evolutions

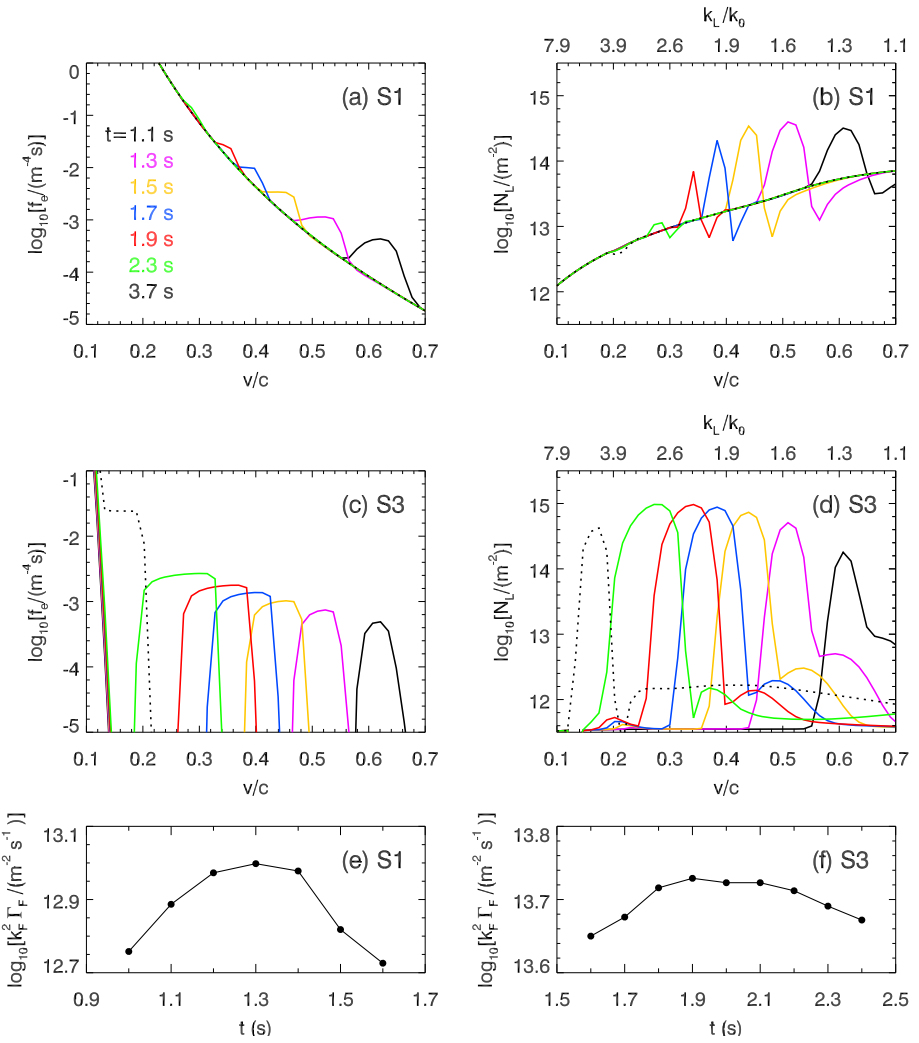

Figure 4 Top and middle rows: snapshots at specific times of phase space distributions $f_e(v)$ (left) and $N_L(v)$ (right) at $x_a = 0.302$ Gm for S1 (top row) and S3 (middle row). Solid curves are for $t = 1.1-2.3$ s, and dotted curves for $t = 3.7$ s. In (b) and (d) the relative wavenumber k_L/k_0 corresponding to v is shown on the top axes, where $k_0 = 2\omega_p c_S/3v_e^2 = 2.2$ m^{-1}. Bottom row: temporal profiles of the maximum $k_F^2\Gamma_F$ at x_a for S1 (left) and S3 (right).

for S1 and S3 of $f_e(x_a, v)$, $N_L(x_a, v)$, and the maximum $k_F^2\Gamma_F(x_a)$. A comparison of Figures 4(a) and 4(c) shows that the beam in S1 is much weaker. Specifically, the beam in S1 has a lower height relative to the background, is narrower and confined to large v only, and is briefer, than the beam in S3. For example, in S1 by the time $t = 2.3$ s the beam feature near $v = 0.28c$ is minimal, while in S3 until $t = 3.7$ s the beam is still not fully relaxed and has $v \approx 0.13-0.18c$. Figures 4(b) and 4(d) show that L_0 waves are enhanced correspondingly, with narrower widths and lower levels of enhancement relatively to thermal in S1 than in S3 except for $t = 1.1$ s. Moreover, we see that the L_0 waves in both cases reach their maxima

at different times, with smaller t (≈ 1.3 s) and so larger v (or smaller k_L) in S1. These occur because of the quantitative differences between the two cases: the much greater number of background electrons at speeds above $\approx 0.1c$ for S1 [see Figure 3(a)], which leads to much smaller beam number density relative to the background and much larger Landau damping rate [see Figure 3(b)], and thus weaker enhancements in N_L and a different time when N_L reaches maximum. Figures 4(b) and 4(d) also show that in S1 the thermal levels $N_{L\theta}(x_a, v)$ of Langmuir waves are higher, because of the greater spontaneous emission dominating stronger damping per Equation (8).

Despite these contrasts, Figures 4(a) – 4(d) also show striking similarities between S1 and S3. Specifically, we see that both beams peak at similar v when they both exist ($t \leq 2.3$ s), and the L_0 waves at the corresponding v are strongest. These similarities are expected, since identical electron injection is imposed for both cases. Consequently, early in the evolution of the beam and L_0 waves, they have large v and small k_L for both S1 and S3. In particular, Figures 4(b) and 4(d) show that $k_L/k_0 \lesssim 2$ for $t \lesssim 1.5$ s, where $k_0 = 2\omega_p c_S/3v_e^2$ (Melrose, 1986; Cairns, 1987a), with $k_0 = 2.2\ \mathrm{m}^{-1}$ here. The wavenumber k_0 strongly affects the rates of ES and EM decays (Cairns, 1987a; Ziebell, Gaelzer, and Yoon, 2001; Kontar and Pecseli, 2002; Li *et al.*, 2003, 2005b) and thus the remote type III emission (*e.g.*, Li, Cairns, and Robinson, 2009).

Figure 4(e) shows that, for S1, $k_F^2\Gamma_F$ peaks at $t \approx 1.3$ s, earlier than $t \approx 1.9$ s for S3 in Figure 4(f). This temporal advance for S1 occurs because at $x = x_a$ the L_0 waves reach their maxima earlier (with larger v or smaller k_L), as discussed above. The corresponding Γ_F thus peaks earlier at smaller k_F, because $k_F \propto k_L$ (Cairns, 1987a). Consequently, the weighted rate $k_F^2\Gamma_F$ reaches its peak value earlier (although k_F is smaller, this is outweighed by the relatively larger values of Γ_F). The radiation in Figure 1(a) thus drifts faster. In contrast, the fast beam electrons in S3 produce at a given frequency much lower levels of f_p fluxes than the peak levels, which are generated by stronger L_0 waves at larger k_L (or smaller v) due to the arrival of the more numerous slower beam electrons later on.

4. Scalings of f_p Spectral Properties with κ for Power-Law Electron Injection

Previous work (*e.g.*, Li, Robinson, and Cairns, 2008; Li, Cairns, and Robinson, 2009, 2011) found that variations in the macroscopic conditions of the background corona [*e.g.*, $n_e(x)$ and $T_e(x)$] affect electron beams and waves in type III sources, and hence the remote type III bursts. Here we explore the effects on the spectral characteristics of f_p emission by varying the κ index of the background particle distributions. Following the predictions of Ko *et al.* (1996) and the suggestions of Maksimovic, Pierrard, and Lemaire (1997), we assume that in the corona κ varies between 4 and 10.

Figure 5 shows the variations with κ of the spectral properties Φ_F^{max}, T_b^{max}, and $\mathrm{d}f/\mathrm{d}t$ at two frequencies $f = 100$ MHz and 60 MHz, and of v_b, for two ranges of the κ index. The characteristic beam speed v_b is obtained by applying Equation (15) to the simulated $\mathrm{d}f/\mathrm{d}t$ results. The v_b values are then checked for consistency and good agreement is found with the simulated beam dynamics, as detailed in Sections 3.2 and 3.3. The left panels of Figure 5 are for $\kappa = 5-10$ and $F_{inj} = 5 \times 10^{-6}$, and the right panels for $\kappa = 4-6$ and $F_{inj} = 5 \times 10^{-5}$, with otherwise identical parameters to those of S1 – S3. Here we parametrize F_{inj} with two different values in order to explore both the small and large κ regimes. This is needed because a given F_{inj} can produce remotely observable f_p emission only for a limited range of κ, and so larger F_{inj} are required for sufficiently smaller κ. Besides showing the scaling results, we also show in Figure 6 predictions from a new simulation, S4, for which

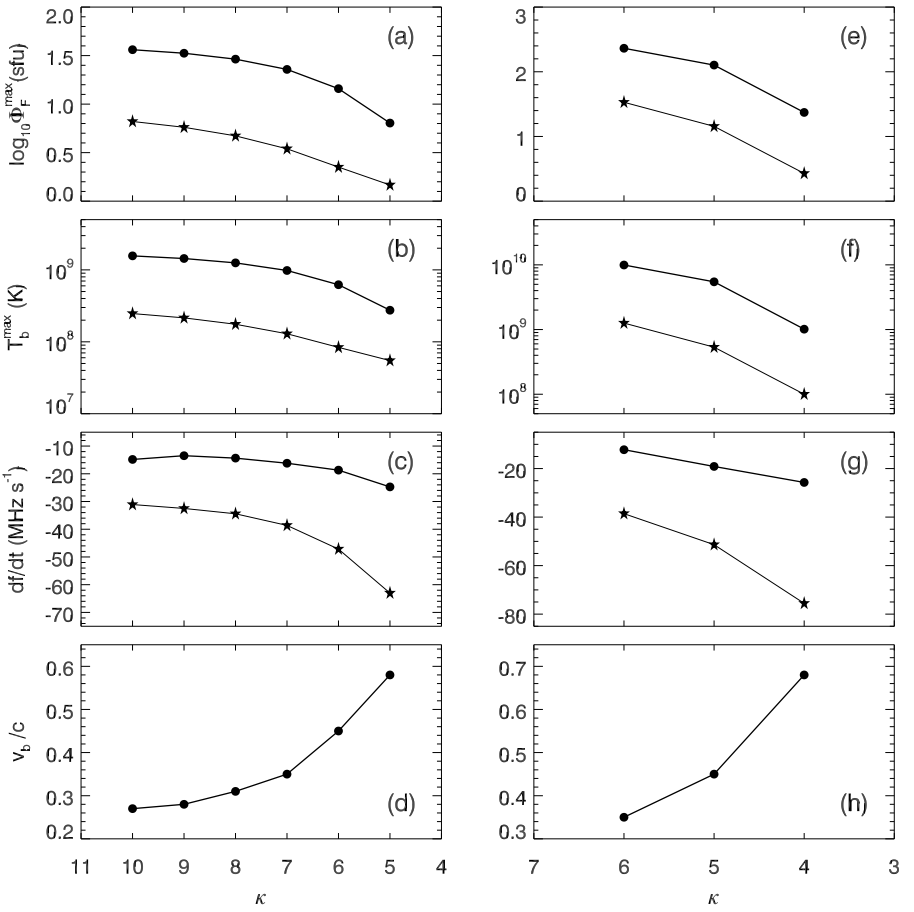

Figure 5 Effects of varying κ on the spectral properties of remotely observed f_p emission for $F_{inj} = 5 \times 10^{-6}$ (left) and $F_{inj} = 5 \times 10^{-5}$ (right) and otherwise identical parameters to S1–S3: Φ_F^{max} (top row), T_b^{max} (second row), and df/dt (third row) at 100 MHz (stars) and 60 MHz (circles), and v_b/c (bottom row).

$F_{inj} = 5 \times 10^{-5}$, a factor of 10 larger than in S1, and the other parameters are identical to those of S1. The characteristic parameters of S4 and its prediction for v_b/c are shown in Table 1.

We see from Figure 5 that as κ decreases Φ_F^{max} and T_b^{max} both decrease while $|df/dt|$ and v_b both increase, for both ranges of $\kappa = 5-10$ (with $F_{inj} = 5 \times 10^{-6}$) and $\kappa = 4-6$ (with $F_{inj} = 5 \times 10^{-5}$). As discussed in Section 3.3 relevant to Figures 4(a) and 4(c), for the same electron injection a smaller κ corresponds to a larger number of background electrons for $v \gtrsim 3v_e$, so the number of beam electrons relative to the background is smaller, and thus the beam is weaker. Furthermore, the beam produced in a smaller κ plasma is above the background distribution only for large, but not for small, values of v. The beam electrons thus have a smaller range of v; in other words, the beam is narrower. The smaller Φ_F^{max} and T_b^{max} for a smaller κ are produced predominantly by the effects of the beam being weaker and narrower and of the Landau damping rate for Langmuir waves being larger, leading

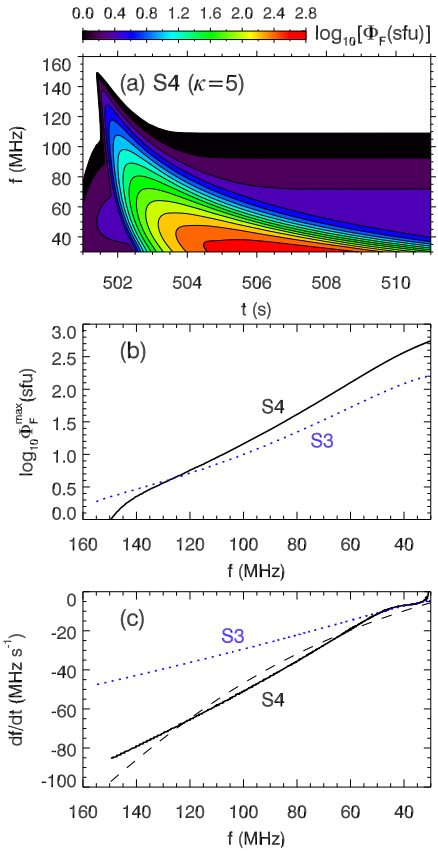

Figure 6 Predictions for S4 with $F_{\rm inj} = 5 \times 10^{-5}$ and otherwise identical parameters to S1: (a) $f_{\rm p}$ dynamic spectrum, and the associated frequency profiles of (b) $\Phi_{\rm F}^{\rm max}$ and (c) $\mathrm{d}f/\mathrm{d}t$. The black dashed curve in (c) is the prediction of Equation (15) for $v_{\rm b} = 0.45c$, while the blue dotted curves in (b) and (c) are for S3.

to smaller $N_{\rm L}$ and so smaller contributions to the emission rate $\Gamma_{\rm F}$. On the other hand, the larger $v_{\rm b}$ and $|\mathrm{d}f/\mathrm{d}t|$ are caused by the fact that the quasi-linearly relaxed beam is faster. Further, the left panels of Figure 5 show that as κ increases all the quantities approach those for S3, where $\kappa \to \infty$. Moreover, Figure 5(h) shows that for the $\kappa = 4$ case $v_{\rm b} \approx 0.68c$, significantly larger than those ($\lesssim 0.25c$) for Mawellian plasmas (Li, Cairns, and Robinson, 2008b, 2009, 2011; Li and Cairns, 2013b).

Figure 5 also shows that, for the two cases of $\kappa = 5$ with the different $F_{\rm inj}$ values, $v_{\rm b}$ and $|\mathrm{d}f/\mathrm{d}t|$ decrease as $F_{\rm inj}$ increases, with $v_{\rm b} = 0.58c$ and $0.45c$ in Figures 5(d) and 5(h), respectively. In contrast, both $\Phi_{\rm F}^{\rm max}$ and $T_{\rm b}^{\rm max}$ increase as $F_{\rm inj}$ increases. These results agree qualitatively with those for Maxwellian plasmas (Li, Cairns, and Robinson, 2009), yet the quantitative changes in $v_{\rm b}$ here are much greater than for the Maxwellian plasmas. Therefore, $v_{\rm b}$ in κ plasmas is more sensitive to $F_{\rm inj}$ variations, especially for small κ, than in Maxwellian plasmas. The reason for the decreasing $v_{\rm b}$ as $F_{\rm inj}$ increases is that as $F_{\rm inj}$ increases, the range of v for which the beam is significantly above the background increases, especially towards the lower end $v_{\rm min}$. Thus, quasi-linear relaxation leads to a slower beam.

Figure 6 shows that for S4 the predicted $f_{\rm p}$ spectrum and the associated spectral properties are qualitatively similar to those for S1. However, quantitatively, the $f_{\rm p}$ emission in Figure 6(a) is much stronger and drifts more slowly than that in Figure 1(a) for S1. For example, Figure 6(b) shows that $\Phi_{\rm F}^{\rm max} \approx 550$ sfu at $f \approx 30$ MHz, in contrast to $\Phi_{\rm F}^{\rm max} \approx 30$ sfu in Figure 1(d) for S1. Moreover, compared with the radiation in Figure 1(c) for S3, this new

burst has a similar onset frequency, yet Φ_F^{max} in S4 increases with decreasing f at a faster rate than in S3. The drift rates in Figure 6(c) indicate that the new beam has $v_b \approx 0.45c$, slower than that for S1 yet much faster than that for S3 (where $v_b \approx 0.25c$). Discussion of the beam and L_0 waves in the source for S4 is deferred to the next section.

5. Further Simulations with Maxwellian Electron Injection

Type III beams can also evolve from injection of thermally heated electrons into the coronal background (Benz, 2002). These electrons may have similar spectral forms to the background electrons, such as the Maxwellian distributions commonly assumed (*e.g.*, Grognard, 1985; Ziebell, Gaelzer, and Yoon, 2001; Benz, 2002; Kontar and Pecseli, 2002; Li, Cairns, and Robinson, 2008a). Here we discuss f_p emission produced in a new simulation, S5, where the injected energetic electrons have

$$I_{Max}(v) = f_h^{Max}(v, T_h), \tag{16}$$

replacing $I_p(v)$ in Equation (14). Here f_h^{Max} is Maxwellian at a flare electron temperature T_h ($\gg T_e$). In S5 we set $T_h = 30$ MK (corresponding to a strong flare), while all the other parameters (*e.g.*, $F_{inj} = 5 \times 10^{-5}$) are identical to those of S4, which assumes power-law injected electrons and a κ background plasma. The characteristic parameters of S5 and its prediction for v_b/c are shown in Table 1.

Figure 7 shows, for S5, the predicted f_p emission spectrum and its spectral properties. On comparing Figure 7 with Figure 6 for S4, we find that the f_p emission in S5 has a lower onset frequency (≈ 135 MHz, *i.e.*, by ≈ 10 %), is weaker except near the lowest simulated frequency (30 MHz), and drifts much more slowly, than in S4. We see from Figure 7(b) that as f decreases Φ_F^{max} increases faster than in S4 for $f \lesssim 80$ MHz, and increases much faster over the whole f-range simulated than in S3 (with Maxwellian background and power-law injected electrons). Furthermore, the drift rates in Figure 7(c) indicate that $v_b \approx 0.30c$ according to Equation (15). This beam speed is thus lower by 50 % than $v_b \approx 0.45c$ in S4, yet is still larger than $v_b \approx 0.25c$ in S3 for the Maxwellian background corona.

To demonstrate the origins of the changes in v_b between S4 and S5, Figure 8 compares the temporal evolutions of $f_e(x_a, v)$ and $N_L(x_a, v)$ for the two cases. We see from Figures 8(a) – 8(d) that the qualitative features of the beams and Langmuir (L_0) waves are similar for S4 and S5. However, quantitatively, the details are different between the two cases. Specifically, we see that the beam in S5 is weaker early ($t < 2.1$ s) in its evolution with lower heights relative to the background, and has smaller v_{max} and larger v_{min}, and thus narrower widths. Moreover, the differences between the two beams become smaller as time progresses. For example, for S5 no beam is visible at $t = 0.9$ s in Figure 8(a) while for S4 at the same time the beam is clearly present in Figure 8(c), whereas both beams are similar at $t = 2.1$ s. By the time $t = 2.4$ s the beam in S5 is actually slightly stronger. The relative changes between the two beams are entirely due to the spectra of injected electrons being different for S4 and S5. In S5, far fewer fast electrons are injected than in S4, due to the much faster fall-off of the Maxwellian spectrum than the power-law spectrum. On the other hand, more slow electrons are injected in S5, since the total numbers of the injected electrons are the same in S4 and S5. The relative differences for the injected fast and slow electrons in S4 and S5 cause the relative differences between the two beams.

The L_0 waves in Figures 8(b) and 8(d) are thus enhanced with different levels and widths, although the differences are minor at $t = 2.1$ s and 2.7 s. In particular, the L_0 waves for

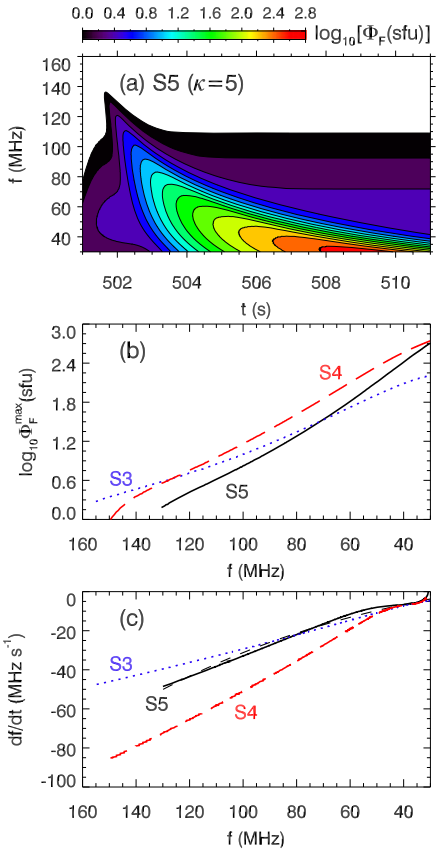

Figure 7 Predictions for S5, which has a Maxwellian injection spectrum (16) with $T_h = 30$ MK and otherwise identical parameters to S4: (a) f_p dynamic spectrum, and the associated frequency profiles of (b) Φ_F^{max} and (c) df/dt. The dashed curve in (c) is the prediction of Equation (15) for $v_b = 0.30c$, in (b) and (c) the dotted and long-dashed curves are for S3 and S4, respectively.

the two cases peak at different times and phase speeds, with $t = 1.5$ s and $v \approx 0.44c$ for S4 and $t = 2.1$ s and $v \approx 0.31c$ for S5. We also found (not shown) that at these times the corresponding $k_F^2 \Gamma_F$ reaches approximately its maxima [*cf.* Figures 4(e) and 4(f)]. The results of $v \approx 0.31c$ and $\approx 0.44c$ for the maximum L_0 waves at $x = x_a$ for S5 and S4, respectively, thus agree with the corresponding beam speeds $v_b \approx 0.30c$ and $0.45c$, which are obtained from the simulated df/dt results and Equation (15). Figure 8(b) also shows that the strong electron injection (with $F_{inj} = 5 \times 10^{-5}$) in S5 enhances the L_0 waves early on ($t \lesssim 1.5$ s) at small wavenumbers ($k_L/k_0 \lesssim 2$), similar to those in Figures 4(b) and 4(d) for S1 and S3, respectively.

Digressing slightly, we now compare the two beams at $t = 1.5$ s in Figures 8(c) and 4(a), which are for S4 with $F_{inj} = 5 \times 10^{-5}$ and S1 with $F_{inj} = 5 \times 10^{-6}$, respectively. We see that at this time the beam in S4 has smaller $v_{min} \approx 0.37c$ and larger $v_{max} \approx 0.48c$ than the beam in S1, which has $v_{min} \approx 0.41c$ and $v_{max} \approx 0.46$. Thus as F_{inj} increases, the width of the beam increases and the beam is shifted more towards small v than towards large v. Quasi-linear relaxation then results in a slower beam for S4 than for S1, as discussed near the end of Section 4.

Returning to Maxwellian injection spectra, further studies show that varying T_h within the range of typical flare temperatures (with the other parameters unchanged) does not affect v_b much. For example, $v_b \approx 0.35c$ for $T_h = 20$ MK and otherwise identical parameters to S5. (For even lower $T_h \lesssim 15$ MK, f_p emission is barely observable.) Therefore, type

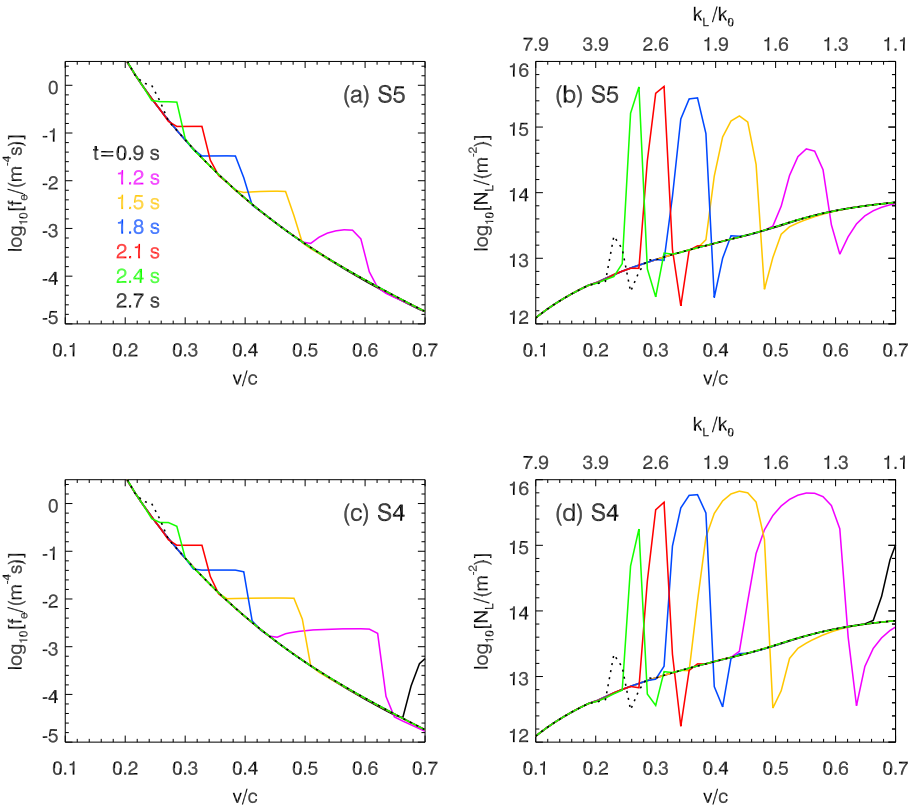

Figure 8 Snapshots at specific times of phase space distributions $f_e(v)$ (left) and $N_L(v)$ (right) at $x_a = 0.302$ Gm for S5 (top) and S4 (bottom). Solid curves are for $t = 0.9-2.4$ s, and dotted curves for $t = 2.7$ s. In (b) and (d) the relative wavenumber k_L/k_0 corresponding to v is shown on the top axes.

III beams produced by Maxwellian injection spectra in κ-distributed coronal plasmas are slower than those produced by power-law injection spectra. Qualitatively similar results are found for Maxwellian-distributed coronal plasmas (Li and Cairns, 2013b). In further detail, our early work for Maxwellian-distributed coronal plasmas showed that $v_b \lesssim 0.2c$ for Maxwellian injection spectra (*e.g.*, Li, Cairns, and Robinson, 2009) and $v_b \lesssim 0.25c$ for power-law injection spectra (Li and Cairns, 2013b).

6. Discussion

The results in Section 3 show that the presence of suprathermal particles in the background corona causes both qualitative and quantitative modifications to type III emission processes. We found that for κ-distributed coronal plasmas the beam-wave and wave-wave interactions in type III bursts take place primarily at large speeds for the beam electrons and thus at large phase speeds and small wavenumbers for the waves. In contrast, the regime of smaller phase speeds and larger wavenumbers is more important for Maxwellian-distributed than κ-distributed corona, as shown in our previous work for Maxwellian electron injections (*e.g.*, Li, Cairns, and Robinson, 2008b, 2009) and is demonstrated here in Section 3 for injected

electrons with power-law spectra. This change in the parametric regimes for the beams and waves in type III sources causes faster type III beams and faster-drifting type III bursts in κ-distributed than Maxwellian-distributed background plasmas. For example, the beam speed $v_b \approx 0.58c$ and $0.25c$ for a $\kappa = 5$ background (S1) and the corresponding Maxwellian background (S3), respectively, for the same injected electrons. Detailed studies further show that the drift rates $\mathrm{d}f/\mathrm{d}t$ of f_p emission produced in a κ-plasma agree quantitatively with Equation (15), for an approximately constant v_b that is consistent with the speeds and dynamics of the beam electrons predicted inside the source region.

We studied further in Section 4 the scalings of the spectral properties of f_p emission with varying κ, for power-law electron injection. We found that as κ decreases v_b and $|\mathrm{d}f/\mathrm{d}t|$ both increase while Φ_F^{max} and T_b^{max} decrease. For example, $v_b \approx 0.45c$ in S4 with $\kappa = 5$ while $v_b \approx 0.68c$ for $\kappa = 4$ and otherwise identical simulation parameters. On the other hand, as κ increases (see the left panels of Figure 5) v_b and the other properties approach the asymptotic limits that are obtained from S3, where $\kappa \to \infty$. Moreover, for predicted f_p emission with similar onset frequencies, the radiation generated in κ-distributed plasmas intensifies much more strongly with decreasing frequency, besides drifting faster, than in Maxwellian-distributed plasmas; see Figure 6(b) for S3 and S4. Therefore, such f_p emission produced in small κ-plasmas can more easily overcome the strong propagation losses, including free-free absorption and scattering-induced damping (Robinson and Benz, 2000; Benz, 2002; Li, Cairns, and Robinson, 2008a), than that produced in Maxwellian plasmas (*e.g.*, Li, Cairns, and Robinson, 2008b; Li and Cairns, 2013b).

Section 5 shows that f_p emission drifts more slowly and v_b is smaller for injection of electrons with Maxwellian spectra into κ-distributed coronal plasmas than for injected electrons with power-law spectra and otherwise the same conditions. For example, $v_b \approx 0.3c$ in S5 for a Maxwellian spectrum, compared with $v_b \approx 0.45c$ in S4 for a power-law spectrum. Nonetheless, such v_b values for Maxwellian injection spectra and κ background plasmas are larger than those ($\lesssim 0.25c$) for Maxwellian background plasmas (*e.g.*, Li, Cairns, and Robinson, 2009; Li and Cairns, 2013b), as shown in Table 1. The reason is that the larger background for κ plasmas prevents beams from relaxing towards smaller v and thus the beams are faster than for Maxwellian plasmas.

The predicted ion sound waves are thermal for the simulation parameters, which are based on observations (*e.g.*, Ko *et al.*, 1996; Aschwanden, 2002; Lin, 2011). This result is the same as that for Maxwellian-distributed coronal plasmas (*e.g.*, Li, Cairns, and Robinson, 2008b). The ion sound waves remain thermal mainly because of the strong damping associated with the relation $T_i \approx T_e$ in the corona (Li, Cairns, and Robinson, 2008b), while the effects of varying the κ index in the background ion distribution $f_i^\kappa(v)$ are unimportant (Thorne and Summers, 1991). Thus the f_p emission is insensitive to the κ index in the background ion distribution $f_i^\kappa(v)$ that affects ion sound waves, in contrast to its strong sensitivity to the κ index (especially for small κ) in the background electron distribution $f_e^\kappa(v)$.

Comparisons with observations of the simulation results from this work (*e.g.*, Table 1) and from our earlier work (*e.g.*, Li, Cairns, and Robinson, 2009) thus suggest the following. i) Fast electron beams with $v_b \gtrsim 0.5c$ associated with the fast-drifting coronal type III bursts sometimes observed (*e.g.*, Wild, Sheridan, and Neylan, 1959; Raoult *et al.*, 1989; Poquérusse, 1994) are produced in regions of the corona where the background electrons have κ distributions with $\kappa \lesssim 5$ and the energetic electrons injected into the corona have power-law spectra. Both conditions are required to produce such fast beams in the corona with observable levels of f_p emission at Earth. ii) The moderately fast-drifting coronal type III bursts observed with $v_b \approx 0.3-0.5c$ are generated in coronal

regions having κ distributions with $\kappa \lesssim 8$, by injecting energetic electrons with either power-law or Maxwellian spectra. iii) Slower type III beams observed with $v_b \lesssim 0.3c$ are generated in coronal regions where the background electrons have Maxwellian distributions or κ distributions with $\kappa > 8$, for either power-law or Maxwellian electron injections. Our suggestion that suprathermal electrons are sometimes present in the background corona and hence in the solar wind is consistent with *in situ* observations (Ko *et al.*, 1996; Maksimovic, Pierrard, and Riley, 1997), and with models for coronal heating (*e.g.*, Scudder, 1992a, 1992b) and solar wind acceleration (*e.g.*, Maksimovic, Pierrard, and Lemaire, 1997). Our simulations and associated comparisons with observations thus support these models from the new viewpoint of nonthermal solar radio emission. In addition, our suggestion that power-law injection spectra for flare-energized electrons are required to account for observations of very fast-drifting type III bursts is consistent with observations of such electrons *in situ* and of X-ray emission (Lin, 1974, 2011).

The qualitative results here for coronal conditions should also be applicable to type III bursts in the solar wind, whose electrons are κ-distributed (*e.g.*, Maksimovic, Pierrard, and Riley, 1997). The κ-distributed solar wind plasmas should support faster type III beams than those for the commonly assumed Maxwellian plasmas. Nevertheless, losses of energy along their paths to Langmuir waves and the ambient plasmas associated with wave-particle interactions and plasma inhomogeneities (*e.g.*, Kontar, 2001; Li, Robinson, and Cairns, 2006; Reid and Kontar, 2010; Ziebell *et al.*, 2011) will slow down the beams gradually as they leave the Sun. These joint effects may lead to the observed slower type III beams in the solar wind (Fainberg, Evans, and Stone, 1972; Lin *et al.*, 1981; Dulk *et al.*, 1987; Graham *et al.*, 2012) than in the corona.

This work predicts only the f_p emission but not the $2f_p$ emission, because our present type III model (Li, Cairns, and Robinson, 2008a; Li, Robinson, and Cairns, 2008) is based on the "head-on" approximation for the coalescence $L + L' \rightarrow H$ that produces $2f_p$ emission, assuming that the L and L' waves are nearly oppositely directed (*e.g.*, Cairns, 1987b; Willes, Robinson, and Melrose, 1996). This approximation is valid when the wavenumbers k_L of Langmuir waves are much greater than those of the H waves, or equivalently $k_L \gg k_0$ (Willes, Robinson, and Melrose, 1996; Li *et al.*, 2005a). Although valid for Maxwellian injection spectra and Maxwellian background plasmas in previous simulations (*e.g.*, Li, Cairns, and Robinson, 2008b; Li and Cairns, 2013b), this approximation breaks down for the power-law injection spectra commonly inferred from observations (Lin, 1974, 2011), as demonstrated in this work, *e.g.*, Figures 4(b) and 4(d). The reason is that the large speeds of the beam electrons early on correspond to small k_L comparable to k_0, and these k_L values are too small to produce $2f_p$ emission via the "head-on" approximation for the coalescence. For example, $v \gtrsim 0.5c$ corresponds to $k_L \lesssim 1.5k_0$. The approximation is also improper in the current simulation S5 [see Figure 8(b)], where the flare plasma is very hot (with $T_h = 30$ MK) and the electron injection is very strong (with $F_{inj} = 5 \times 10^{-5}$) so that many fast electrons are injected and the beam electrons with $v > 0.5c$ have sizable effects in producing the radiation. In order to predict the $2f_p$ emission properly, future work should remove the "head-on" restriction to allow contributions associated with small k_L, in which the L and L' waves can have wave vectors in approximately the same direction (Willes, Robinson, and Melrose, 1996).

Finally, we consider an alternative representation of the suprathermal background particles assumed in this work. It is common to approximate the presence of suprathermal particles in the solar wind by a sum of two Maxwellian distributions at different temperatures T_m

(*e.g.*, Feldman *et al.*, 1975; Maksimovic, Pierrard, and Riley, 1997; Zouganelis *et al.*, 2004):

$$f_{1D}^{\kappa}(v) = \sum_{m>1}^{M} \alpha_m f_m^{\mathrm{Max}}(v, T_m), \tag{17}$$

where $\alpha_m < 1$ represents the fractional contribution of the component m. However, for our simulations with suprathermal background particles having speeds extending to $\approx c$, the upper bound M in Equation (17) would be much greater than 1, since a single Maxwellian distribution falls off exponentially with energy and can only fit a limited v-range of the background. For example, for the $\kappa = 5$ background (as in Figure 3(a) for S1), a Maxwellian component with $T_m \approx 200$ MK and $\alpha_m \approx 3 \times 10^{-8}$ would be required to approximate the suprathermal background electrons at $v/c \approx 0.50-0.65$, and a larger T_m would be needed for $v/c \gtrsim 0.65$. The existence of Maxwellian distributions at such large T_m values in the corona appears unlikely, according to the recent hard X-ray spectral and imaging data (Lin, 2011), although historically thermal temperatures with 10^{8-9} K were suggested (Crannell *et al.*, 1978; Elcan, 1978) due to poorer data quality. Therefore, the simple representation in our simulations of the coronal suprathermal background electrons with a κ distribution appears efficient, justifiable, and effective in producing fast coronal type III beams.

7. Conclusions

We have presented the first detailed, quasi-linear-based simulations to study f_p emission of type III bursts produced in the corona with non-Maxwellian, suprathermal distributions of background plasmas. The coronal background particles are assumed to have kappa (κ) distributions with suprathermal tails, as inferred from solar wind data and suggested by models for heating of the corona and acceleration of the solar wind (see the review by Pierrard and Lazar, 2010). The type III electron beams are formed by time-of-flight effects for time- and position-localized injections of fast electrons during flares with power-law or Maxwellian spectra. We find that the assumption of suprathermal background particles leads to major qualitative progress in understanding type III bursts and resolves longstanding problems with the productions of type III beams with beam speeds of $v_b > 0.25c$. The additional assumption of power-law injection spectra is vital for producing the fastest type III beams ($v_b > 0.5c$) inferred from observations.

Specifically, the simulations show that coronal regions with suprathermal background plasma (especially with small κ indices) can produce significantly faster type III beams and faster drifting f_p emission than for thermal Maxwellian background plasma, for flare-energized electrons with power-law or Maxwellian injection spectra. We emphasize that the v_b values predicted from the drift rates of f_p emission according to Equation (15) agree well with the dynamics of beam electrons and waves in the radio source. We find that production of type III beams with $v_b \gtrsim 0.3c$ requires that the coronal background plasmas have κ distributions with $\kappa \lesssim 8$, for both power-law and Maxwellian electron injection spectra. Moreover, beams with $v_b \gtrsim 0.5c$ also require power-law electron injection, not Maxwellian electron injection. In detail, for identical power-law injection spectra, simulations S1 and S3 yield $v_b \approx 0.58c$ and $0.25c$, respectively (see Table 1), for identical profiles of the coronal density and temperature, differing only in that the background particles are κ-distributed ($\kappa = 5$) and Maxwellian-distributed, respectively. Furthermore, $v_b \approx 0.3-0.35c$ for injected electrons with Maxwellian spectra for typical flare temperatures (*e.g.*, see S5 in Table 1) and otherwise identical coronal conditions to S1, and these v_b values are smaller than those for

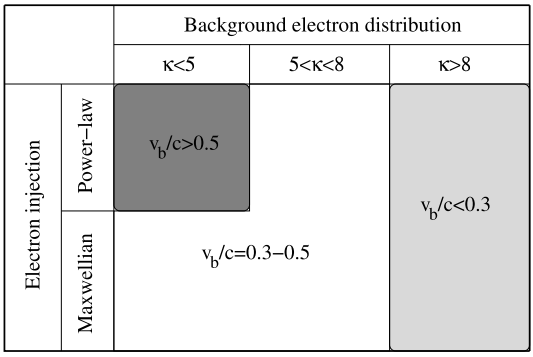

Figure 9 Schematic summary of the predicted dependence of type III beam speed v_b/c on the κ value of the background electron distribution function and on the spectral form of the injected energetic electrons.

the power-law spectra. These beams produced in small-κ background plasmas are thus faster than those (with $v_b \lesssim 0.25c$) generated in Maxwellian background plasmas for coronal parameters (*e.g.*, Li, Cairns, and Robinson, 2008b; Li and Cairns, 2013b). Figure 9 summarizes our simulation results schematically.

The simulations also show that, for similar radiation onset frequencies, besides drifting faster, the f_p emission produced in small-κ background plasmas intensifies more strongly with decreasing frequency than in Maxwellian backgrounds. Such f_p emission produced in small-κ coronal plasmas is thus able to more easily overcome strong losses during propagation, including free-free absorption (Benz, 2002) and scattering-induced damping (Robinson and Cairns, 1998; Li, Cairns, and Robinson, 2008a), than that in Maxwellian-distributed corona (*e.g.*, Li and Cairns, 2013b).

The modifications to f_p emission observable at Earth when suprathermal background particles are present in the corona are manifestations of changes in the radiation processes in the source, and are not due to changes in propagation of radiation, which is independent of the microscopic details of the background particle distributions (Li, Cairns, and Robinson, 2008a). Strong beams are present at larger v in κ-distributed than in Maxwellian-distributed plasmas. This happens because there is a positive slope in the electron distribution function, and thus a beam only develops at large v in κ-distributed plasmas, due to the much higher levels of background distribution there than in Maxwellian plasmas. Quasi-linear relaxation then naturally leads to a faster beam for the κ cases compared to the Maxwellian cases. Because the beam electrons in κ-distributed plasmas have larger v, the wave-wave interactions leading to f_p emission take place at larger phase speeds v and smaller wavenumbers k. Further, the values of v are larger for injected electrons with power-law spectra than for Maxwellian spectra, since a power-law injection provides more fast electrons as the source of a type III beam. Thus, the associated type III bursts drift faster. On the other hand, in Maxwellian-distributed coronal plasmas the radiation processes operate from large v and small k to small v and large k. However, strong beams and waves develop at smaller v and larger k for a Maxwellian background, due to the operation of quasi-linear relaxation at smaller v for the weaker Maxwellian background than for a κ background. The dominance of these strong beams and waves consequently produces slower type III beams and more slowly drifting type III bursts than those in κ-distributed corona.

We also find that the ion sound waves participating in type III processes are essentially thermal for the assumed coronal conditions. This occurs primarily due to the strong damping associated with $T_i \approx T_e$ (Li, Cairns, and Robinson, 2008b). In contrast, the effects of varying the κ index in the background ion distribution, which affects ion sound waves, are unimportant (Thorne and Summers, 1991). Therefore, the f_p emission is insensitive to the κ

index for background ions, in contrast to its strong sensitivity to the κ index for background electrons.

Our simulations thus suggest that:

- Fast-drifting coronal type III bursts with $v_b \gtrsim 0.5c$ sometimes inferred from drift rates and source motions (*e.g.*, Wild, Sheridan, and Neylan, 1959; Raoult *et al.*, 1989; Poquérusse, 1994) are produced in coronal regions whose background electrons have κ distributions with $\kappa \lesssim 5$ by flare-energized electrons with power-law injection spectra.
- Moderately fast type III beams with $v_b \approx 0.3 - 0.5c$ are generated in κ-distributed coronal regions with $\kappa \lesssim 8$, by injected electrons with either power-law or Maxwellian spectra.

Consequently, this work supports, from the viewpoint of nonthermal type III emission, the following:

- The presence, at least sometimes, of suprathermal electrons in the background corona. Our results thus are consistent with *in situ* observations (Ko *et al.*, 1996; Maksimovic, Pierrard, and Riley, 1997) and support models for coronal heating and solar wind acceleration that involve suprathermal background distributions (Scudder, 1992a; Maksimovic, Pierrard, and Lemaire, 1997).
- Power-law spectra for injected electrons when fast type III beams with $v_b \gtrsim 0.5c$ are produced. This spectral form and its spectral parameters are consistent with those inferred from *in situ* electron data and X-ray data (Lin, 1974, 2011).

Furthermore, the results from this paper and our previous work (*e.g.*, Li, Cairns, and Robinson, 2009) suggest that the relatively slow type III beams observed with $v_b < 0.3c$ are produced in coronal regions with Maxwellian or κ (> 8) electron distributions, irrespective of whether the injected electrons have power-law or Maxwellian spectra.

Finally, the present results for coronal conditions should also be applicable to f_p emission of type III bursts produced in the solar wind (*e.g.*, Fainberg and Stone, 1974). In the future, the simulations should be generalized to predict $2f_p$ emission, by including extra contributions from pairs of Langmuir waves with small wavenumbers ($k_L \lesssim k_0$), where the pairs are associated with fast beam electrons and propagate in approximately the same direction (Willes, Robinson, and Melrose, 1996). It is also important that relativistic effects be considered in future work on very fast beams ($v_b > 0.5c$), which produce normal type III bursts (*e.g.*, Wild, Sheridan, and Neylan, 1959) and type IIId bursts (*e.g.*, Poquérusse, 1994).

Acknowledgements The authors thank Professor Don Melrose for valuable discussions and the referee for constructive comments. This work was supported by the Australian Research Council via grant DP110101587.

Appendix: Spontaneous Emission of Langmuir and Ion Sound Waves

The spontaneous emission coefficient α_M for wave mode M is related to the three-dimensional particle distribution function $f(\mathbf{p})$ via (Melrose, 1986)

$$\alpha_M(\mathbf{k}) = \int \mathrm{d}^3\mathbf{p} w_M(\mathbf{k}, \mathbf{p}) f(\mathbf{p}), \tag{18}$$

where $\mathbf{p} = m\mathbf{v}$ is the particle momentum, and

$$w_M(\mathbf{k}, \mathbf{p}) = \frac{2\pi e^2 R_M(\mathbf{k})}{\epsilon_0 \hbar |\omega_M(\mathbf{k})|} \left|\mathbf{e}_M^*(\mathbf{k}) \cdot \mathbf{v}\right|^2 \delta\left\{\omega_M(\mathbf{k}) - \mathbf{k} \cdot \mathbf{v}\right\}. \tag{19}$$

Here $\mathbf{e}_{\mathrm{M}}(\mathbf{k})$ is the unit electric vector of the wave mode M, and $R_{\mathrm{M}}(\mathbf{k})$ represents the ratio of electric to total energy in the M mode, with (Melrose, 1986)

$$R_{\mathrm{L}}(\mathbf{k}) = \frac{1}{2}\left[\frac{\omega_{\mathrm{L}}(\mathbf{k})}{\omega_{\mathrm{p}}}\right]^2, \tag{20}$$

$$R_{\mathrm{S}}(\mathbf{k}) = \frac{1}{2}\left[\frac{\omega_{\mathrm{S}}(\mathbf{k})}{\omega_{\mathrm{pi}}}\right]^2, \tag{21}$$

for Langmuir and ion sound waves, respectively, where $\omega_{\mathrm{pi}} = (n_{\mathrm{e}}e^2/m_{\mathrm{i}}\varepsilon_0)^{1/2}$ is the ion plasma frequency. Applying the isotropic three-dimensional κ distributions corresponding to Equation (1) to Equations (18) – (21) and using the dispersion relations [Equations (4) and (5)], we obtain the spontaneous emission rates given by Equations (6) and (7).

References

Allen, C.W.: 1947, *Mon. Not. Roy. Astron. Soc.* **107**, 426.
Aschwanden, M.J.: 2002, *Space Sci. Rev.* **101**, 1.
Bastian, T.S., Benz, A.O., Gary, D.E.: 1998, *Annu. Rev. Astron. Astrophys.* **36**, 131.
Benz, A.O.: 2002, *Plasma Astrophysics: Kinetic Processes in Solar and Stellar Coronae*, 2nd edn., Kluwer Academic, Dordrecht, 32 – 35, 92, 93, 262 – 264, 273 – 276.
Cairns, I.H.: 1987a, *Phys. Plasmas* **38**, 169.
Cairns, I.H.: 1987b, *Phys. Plasmas* **38**, 179.
Cairns, I.H.: 2000, *Phys. Plasmas* **7**, 4901.
Coles, W.A., Harmon, J.K.: 1989, *Astrophys. J.* **337**, 1023.
Crannell, C.J., Frost, K.J., Saba, J.L., Maetzler, C., Ohki, K.: 1978, *Astrophys. J.* **223**, 620.
Decker, R.B., Krimigis, S.M., Roelof, E.C., Hill, M.E., Armstrong, T.P., Gloeckler, G., Hamilton, D.C., Lanzerotti, L.J.: 2005, *Science* **309**, 5743.
Dulk, G.A., Steinberg, J.L., Hoang, S., Goldman, M.V.: 1987, *Astron. Astrophys.* **173**, 366.
Elcan, M.J.: 1978, *Astrophys. J. Lett.* **226**, L99.
Fainberg, J., Evans, L.G., Stone, R.G.: 1972, *Science* **178**, 743.
Fainberg, J., Stone, R.G.: 1974, *Space Sci. Rev.* **16**, 145.
Feldman, W.C., Asbridge, J.R., Bame, S.J., Montgomery, M.D., Gary, S.P.: 1975, *J. Geophys. Res.* **80**, 4181.
Gloeckler, G., Geiss, J., Fisk, L.A.: 2001, In: Balogh, A., Marsden, R.G., Smith, E.J. (eds.) *The Heliosphere near Solar Minimum: The Ulysses Perspective*, Springer, London, 287.
Gloeckler, G., Hamilton, D.C.: 1987, *Phys. Scr.* **T18**, 73.
Graham, D.B., Cairns, I.H., Prabhakar, D.R., Ergun, R.E., Malaspina, D.M., Bale, S.D., Goetz, K., Kellogg, P.J.: 2012, *J. Geophys. Res.* **117**, A09107.
Grognard, R.J.M.: 1985, In: McLean, D.J., Labrum, N.R. (eds.) *Solar Radiophysics*, Cambridge Univ. Press, Cambridge, 253.
Kim, E.-H., Cairns, I.H., Robinson, P.A.: 2008, *Phys. Plasmas* **15**, 102110.
Klassen, A., Karlicky, M., Mann, G.: 2003, *Astron. Astrophys.* **410**, 307.
Klein, K.-L., Krucker, S., Trottet, G., Hoang, S.: 2005, *Astron. Astrophys.* **431**, 1047.
Ko, Y.K., Fisk, L.A., Gloeckler, G., Geiss, J.: 1996, *Geophys. Res. Lett.* **23**, 2785.
Kontar, E.P.: 2001, *Astron. Astrophys.* **375**, 629.
Kontar, E.P., Pecseli, H.L.: 2002, *Phys. Rev. E* **65**, 066408.
Krimigis, S.M., Carbary, J.F., Keath, E.P., Bostrom, C.O., Axford, W.I., Gloeckler, G., Lanzerotti, L.J., Armstrong, T.P.: 1981, *J. Geophys. Res.* **86**, 8227.
Layden, B., Percival, D.J., Cairns, I.H., Robinson, P.A.: 20011, *Phys. Plasmas* **18**, 022309.
Li, B., Cairns, I.H.: 2012, *Astrophys. J.* **753**, 124.
Li, B., Cairns, I.H.: 2013a, *Astrophys. J. Lett.* **756**, L34.
Li, B., Cairns, I.H.: 2013b, *J. Geophys. Res.*, submitted. ID: 2013JA018787.
Li, B., Cairns, I.H., Robinson, P.A.: 2008a, *J. Geophys. Res.* **113**, A06104.
Li, B., Cairns, I.H., Robinson, P.A.: 2008b, *J. Geophys. Res.* **113**, A06105.
Li, B., Cairns, I.H., Robinson, P.A.: 2009, *J. Geophys. Res.* **114**, A02104.
Li, B., Cairns, I.H., Robinson, P.A.: 2011, *Astrophys. J.* **730**, 20.

Li, B., Robinson, P.A., Cairns, I.H.: 2006, *Phys. Plasmas* **13**, 092902.
Li, B., Robinson, P.A., Cairns, I.H.: 2008, *J. Geophys. Res.* **113**, A10101.
Li, B., Willes, A.J., Robinson, P.A., Cairns, I.H.: 2003, *Phys. Plasmas* **10**, 2748.
Li, B., Willes, A.J., Robinson, P.A., Cairns, I.H.: 2005a, *Phys. Plasmas* **12**, 012103.
Li, B., Willes, A.J., Robinson, P.A., Cairns, I.H.: 2005b, *Phys. Plasmas* **12**, 052324.
Li, B., Cairns, I.H., Yan, Y.H., Robinson, P.A.: 2011, *Astrophys. J. Lett.* **738**, L9.
Lin, R.P.: 1974, *Space Sci. Rev.* **16**, 189.
Lin, R.P.: 2011, *Space Sci. Rev.* **159**, 421.
Lin, R.P., Potter, D.W., Gurnett, D.A., Scarf, F.L.: 1981, *Astrophys. J.* **251**, 364.
Liu, C., Lee, J., Karlicky, M., Choudhary, D.P., Deng, N., Wang, H.: 2009, *Astrophys. J.* **703**, 757.
Magelssen, G.R., Smith, D.F.: 1977, *Solar Phys.* **55**, 211.
Maksimovic, M., Pierrard, V., Lemaire, J.F.: 1997, *Astron. Astrophys.* **324**, 725.
Maksimovic, M., Pierrard, V., Riley, P.: 1997, *Geophys. Res. Lett.* **24**, 1151.
Malaspina, D.M., Cairns, I.H., Ergun, R.E.: 2010, *J. Geophys. Res.* **115**, A01101.
Marsch, E.: 2006, *Living Rev. Solar Phys.* 3(1). http://solarphysics.livingreviews.org/Articles/lrsp-2006-1/.
Melrose, D.B.: 1986, *Instabilities in Space and Laboratory Plasmas*, Cambridge Univ. Press, Cambridge, 23 – 25, 80, 84 – 86, 91 – 96.
Meyer-Vernet, N.: 2001, *Solar Phys.* **49**, 247.
Pick, M., Vilmer, N.: 2008, *Astron. Astrophys. Rev.* **16**, 1.
Pierrard, V., Lazar, M.: 2010, *Solar Phys.* **267**, 153.
Pierrard, V., Lemaire, J.: 1996, *J. Geophys. Res.* **101**, 7923.
Poquérusse, M.: 1994, *Astron. Astrophys.* **286**, 661.
Raoult, A., Lantos, P., Klein, K.L., Correla, E., Kaufmann, P.: 1989, *Solar Phys.* **120**, 125.
Reid, H.A.S., Kontar, E.P.: 2010, *Astrophys. J.* **721**, 864.
Reid, H.A.S., Vilmer, N., Kontar, E.P.: 2011, *Solar Phys.* **529**, A66.
Riddle, A.C.: 1974, *Solar Phys.* **35**, 153.
Robinson, P.A., Benz, A.O.: 2000, *Solar Phys.* **194**, 345.
Robinson, P.A., Cairns, I.H.: 1993, *Solar Phys.* **154**, 335.
Robinson, P.A., Cairns, I.H.: 1998, *Solar Phys.* **181**, 363.
Scudder, J.D.: 1992a, *Astrophys. J.* **398**, 299.
Scudder, J.D.: 1992b, *Astrophys. J.* **398**, 319.
Steinberg, J.L., Aubier-Giraud, M., Leblanc, Y., Boischot, A.: 1971, *Astron. Astrophys.* **10**, 362.
Subramanian, P., Cairns, I.H.: 2011, *J. Geophys. Res.* **116**, A03104.
Summers, D., Thorne, R.M.: 1991, *Phys. Fluids B* **3**, 1835.
Suzuki, S., Dulk, G.A.: 1985, In: McLean, D.J., Labrum, N.R. (eds.) *Solar Radiophysics*, Cambridge Univ. Press, Cambridge, 289.
Thejappa, G., MacDowall, R.J.: 2008, *Astrophys. J.* **676**, 1338.
Thorne, R.M., Summers, D.: 1991, *Phys. Fluids B* **3**, 2117.
Tsiklauri, D.: 2011, *Phys. Plasmas* **18**, 052903.
Vasyliunas, V.M.: 1968, *J. Geophys. Res.* **73**, 2839.
Wild, J.P.: 1950, *Aust. J. Sci. Res., Ser. A* **3**, 541.
Wild, J.P., Sheridan, K.V., Neylan, A.A.: 1959, *Aust. J. Phys.* **12**, 369.
Willes, A.J., Robinson, P.A., Melrose, D.B.: 1996, *Phys. Plasmas* **3**, 149.
Zaheer, S., Murtaza, G., Shah, H.A.: 2004, *Phys. Plasmas* **11**, 2246.
Ziebell, L.F., Gaelzer, R., Yoon, P.H.: 2001, *Phys. Plasmas* **9**, 3982.
Ziebell, L.F., Yoon, P.H., Pavan, J., Gaelzer, R.: 2011, *Astrophys. J.* **727**, 16.
Zouganelis, I., Maksimovic, M., Meyer-Vernet, N., Lamy, H., Issautier, K.: 2004, *Astrophys. J.* **606**, 542.